國　立　交　通　大　學

多媒體工程研究所

碩士論文

自動擷取並量化神經細胞影像的型態特徵

Automatic Extraction and Quantification of Morphological Features from Neuron Images

研 究 生：柯志錡

指導教授：陳玲慧　教授

指導教授：何信瑩　教授

中 華 民 國 一 百 零 二 年 七 月

自動擷取並量化神經細胞影像的型態特徵

Automatic Extraction and Quantification of Morphological Features from Neuron Images

研 究 生：柯志錡　　Student：Chih-Chi Ke

指導教授：陳玲慧　　Advisor：Ling-Hwei Chen

指導教授：何信瑩　　Advisor：Shinn-Ying Ho

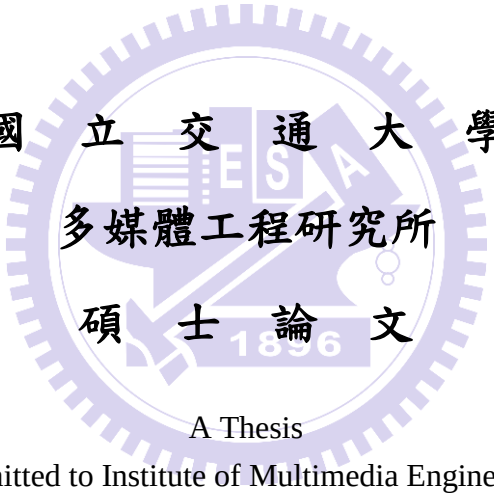

國 立 交 通 大 學

多媒體工程研究所

碩 士 論 文

A Thesis

Submitted to Institute of Multimedia Engineering

College of Computer Science

National Chiao Tung University

in partial Fulfillment of the Requirements

for the Degree of

Master

In

Computer Science

July 2013

Hsinchu, Taiwan, Republic of China

中 華 民 國 一 百 零 二 年 七 月

自動擷取並量化神經細胞影像的型態特徵

學生：柯志錡　　指導教授：陳玲慧 博士

何信瑩 博士

國立交通大學多媒體工程研究所碩士班

摘　要

神經細胞型態的分析對於研究神經細胞的架構和功能之間的關係很重要。為了避免於大量神經細胞影像中費力且漫長的型態特徵分析，以電腦輔助的系統不可或缺。在神經細胞型態中，神經軸結構(如第一神經軸、第二神經軸)的辨認能表徵實驗調節後產生的差異。為了分析神經軸結構，基礎神經細胞型態偵測以及神經軸分枝次序決定是必需的。基礎神經細胞型態，如細胞本體、神經軸，的偵測已被廣泛研究，然而，神經軸分枝次序決定的研究僅有少數。商業軟體 HCA-Vision 是其中最傑出的研究之一。本研究發展出 NeurphologyS，一個可從稀疏染色神經細胞之影像自動擷取並量化型態特徵的系統。提出之系統可自動化量化由五個子集組成的 53 個型態特徵，其中包含神經軸結構特徵。為了做到神經軸分枝次序決定，我們提出了一個基於規則的神經軸增長以及反向分枝優先順序決定的方法(RANBO)。RANBO 包含兩個步驟：1) 基於區域神經軸角度規則的神經軸樹增長 2) 反向的神經軸分枝優先順序決定及分枝次序指派。兩個影像資料集被用以評估提出之系統，其一為經綠色螢光蛋白轉染之海馬迴神經細胞影像，另一為可在 HCA-Vision 網站上取得的 Sez-6 knockout 皮質神經細胞影像。由量化結果可知，提出之系統具備如同 HCA-Vision 的區分神經分枝微妙改變之能力；而提出之系統在神經軸結構的量化方面與 HCA-Vision 相較下表現良好。以 MATLAB 實作之 NeurphologyS 是開放源碼的且可無償取得。

Automatic Extraction and Quantification of Morphological Features from Neuron Images

Student：Chih-Chi Ke　　Advisor：Dr. Ling-Hwei Chen

Dr. Shinn-Ying Ho

Institute of Multimedia Engineering

National Chiao Tung University

ABSTRACT

Analysis of neuronal morphology is crucial for studying the relation between structure and function of neurons. For avoiding laborious and tedious manual analysis of morphological features of massive neuron images, a computer-aided system is indispensable. Out of neuronal morphologies, identification of neurite structure such as primary neurites or secondary neurites can characterize the differences after experimental modulation. For analysis of neurite structure, detection of basic neuronal morphologies and neurite branch order decision is necessary. Detection of basic neuronal morphology (such as soma or neurite) has been well studied, however, there are few studies that can achieve neurite branch order decision. The commercial software, HCA-Vision, is one of the most outstanding studies. This study develops NeurphologyS, a system to automatically extract and quantify morphological features from images of sparsely stained neurons. With the proposed system, 53 morphological features categorized into 5 subsets, can be quantified automatically. For neurite branch order decision, a rule-based neurite tree growing and backward branch priority decision (RANBO) is proposed. RANBO has two steps: 1) neurite tree growing based on

local neurite angle rules 2) backward decision of neurite branch priority and branch order assignment. Two image datasets are utilized to evaluate the proposed system, one is image dataset of GFP transfected hippocampal neurons, and the other is the Sez-6 knockout cortical neuron image dataset available on HCA-Vision website. It can be known from our quantification results that the proposed system possesses the ability to differentiate subtle changes in neurite branching as HCA-Vision, and that the proposed system performs well compared to HCA-Vision in the quantification of neurite structure. The MATLAB-implemented NeurphologyS is open-source and freely available.

ACKNOWLEDGEMENT

首先要感謝陳玲慧博士與何信瑩博士兩位老師在我就讀碩士這兩年間的指導，不論學識上的教導，即使是生活經驗的分享、對學術研究的熱情或為人處世的方式，很多層面都同樣獲益良多。謝謝李建興老師在報告技巧及研究方式的指導，對缺乏研究、報告經驗的我來說非常受用。謝謝黃慧玲老師給予研究上的鼓勵和協助，還有總是非常友善的黃兆祺老師充實了許多我所缺乏的相關知識。

在兩個不同領域的實驗室打轉是難得的經驗，能夠接觸到許多不同的人、事、物，觀察思考的異同並與許多學長姊、同學、學弟妹交流。感謝自動化資訊處理實驗室的成員們，Jimmy 學長、超哥學長、阿和學長、阿三學長、盈如學姊、阿嘉、阿昌、佩庭、阿 Din、阿豪，在會議室裡渡過的每個禮拜一，每個人報告的身影以及討論上的你來我往應該會是我碩士生活中難忘的記憶。還有智慧型計算實驗室的成員們，小雄學長、Burnz 學長、明儒學長、國慶學長、佳達學長、凱迪學長、宇清、乙念、Judy、芳盈，真可說是同甘苦共患難,能夠一起吃大餐也能夠一起趕 project。還有已畢業的學長姐們：子杰、厚邑、維綱、韻如、銘鑫、冠維、馨云，謝謝你們帶領我熟悉兩個實驗室，總會很想念你們仍在的時光。此外要感謝陳文馨學姊在實驗研究的多次協助!

另外要感謝國樂社的大朋友小朋友們，在有時煩悶的新竹研究生活中，也還有一個溫暖的歸處。同是研究生的至鼎、詠翔，平時受到你們很多照顧，希望能夠一起順利取得學位。謝謝總是貪婪的聚餐揪團的老人們，我也即將要邁入職場生活，說不定不久後就會跟你們一起抱怨老闆了。

最重要的，感謝我的家人們在我就學期間的幫助，能讓我無後顧之憂的專心研究。雖然長時間待在新竹，在家的時間少了，但是當我內心疲憊需要休息的時候，回家的念頭總是很強烈。希望家裡的小成員寬寬能順利成長!

最後，謹以此篇論文獻給所有上述的、以及所有關心我的人們。

CONTENTS

LIST OF TABLES

LIST OF FIGURES

CHAPTER 1

INTRODUCTION

1.1 Motivation

The development of fluorescent microscopy facilitates high-throughput neuron image acquisition. In the domain of neuroscience, neuronal morphology plays an important role. Discovery of novel molecular pathway or pharmacological discovery will benefit from quantitative analysis of massive amount of neuron images.

However, analysis of neuron images is labor-intensive and time-consuming. In addition, manual analysis of massive amount of images is unrealistic and prone to bias. Hence, development of computer-aided morphological feature extraction and quantification from neuron images is indispensable.

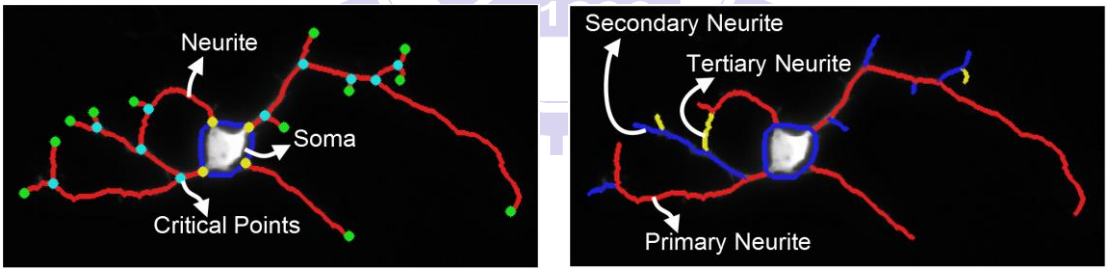

(a) (b)

Fig. 1 An example of neuronal morphologies.

(a) Basic neuronal morphologies. (b) Neurite structure.

To date, most computer-aided methods possess the ability to extract basic neuronal morphologies. Here we refer to cell body (soma), neurite and critical points as basic neuronal morphologies (Fig. 1 (a)). Moreover, we do not distinguish axons and dendrites, and the term neurite is adopted. Despite the importance of neurite, simple metrical measurements such as total neurite length or mean neurite length do

not always have discriminating power for morphological differences [1, 2]. Hence the more detailed description of neurite concerning its structure is required.

To describe structure of neurite, extraction and quantification of neurites with different branch orders is a well-employed approach. Neurites with different branch orders, such as primary neurites elongating from soma directly, secondary neurites sprouting from primary neurites, tertiary neurites sprouting from secondary neurites and so on, are referred to as neurite structure in this study (Fig. 1 (b)). Neurite structure has been widely analyzed in various topics of neuroscience [2-9] including pathway discovery, neural regeneration, neurite growth mechanism etc. However, most of them adopt manual or semi-automatic tracing.

Automatic extraction of neurite structure consists of basic neuronal morphology detection and neurite branch order decision. Detection of basic neuronal morphologies has been well studied. However, although neurite structure is important, to our knowledge, there are few studies that can analyze neurite structure [10-23]. Thus, in this thesis, we propose an automatic system for extraction and quantification of neuronal morphological features, including neurite structure features.

1.2 Related Works

In this section, the related works are arranged into two subsections, one is about how neurite structure features are utilized in various topics of neuroscience and the other is about computer-aided methods for 2D neuron image analysis.

1.2.1 Applications of Neurite Structure in Neuroscience

Gene modulation or pharmacological perturbation might induce morphological differentiations in neuron cells. Neurite length, out of the neuronal morphologies, has been well-studied for characterizing these differences. However, neurite length cannot reflect all morphological changes [1, 2].

Except for neurite length, neurite structure is known to be one of the neuronal morphologies that can characterize neuronal growth. The versatile neurite structure is employed in many studies. For analysis of neurite structure, decision of neurite branch order is necessary. By definition, primary neurites are neurites elongating directly from soma, secondary neurites are neurites sprouting from primary neurites and so on.

Table 1 summarizes the studies that will be mentioned below, and how neurite structure features work. For instance, [2] found that independent of axon outgrowth, axon branching in response to guidance cues can occur over different time courses by different cellular mechanisms; [3] showed that the PI3K-Akt-mTOR signaling pathway promotes the growth and branching of dendrites in cultured hippocampal neurons; [4] demonstrated a role for locally synthesized actin-binding protein β-thymosin in the regulation of normal patterns of neurite outgrowth; [5] investigated an approach demonstrating the ability to combine gene delivery with physical guidance and can be tailored to target specific axonal populations; [6] suggested that to the dichotomy in medium spiny neurons, dendritic area was a major contributor to the dichotomy in electrophysiological properties; [7] compares the results obtained for dendritic branching and predominant dendritic spatial distribution in both subnuclei of male rats and diestrus female rats; [8] suggested that FRMD7 is involved in multiple aspects of neuronal development and has direct importance to further understanding the pathogenesis of IIN; [9] found that secreted ligand Reelin promotes directional growth into marginal zone, an otherwise exclusion zone of L6 neurites.

Table 1 Neurite structure related applications.

Author	How neurite structure employed	
Dent et al. (2004)	**Number and length of primary branch** and total axon length of neuron cultures treating different guidance cues, or the same guidance cue with different doses were compared.	[2]
Jaworski et al. (2005)	**Higher-order (secondary and tertiary) dendrite length** was compared for effect of rapamycin-treating and mTOR knockdown neuron cultures.	[3]
Kesteren et al. (2006)	**Mean lengths of primary neurites** of intact cultures with/without dsRNA inhibition of β-thymosin were compared, while total neurite lengths of transected neurites were compared.	[4]
Houchin-Ray et al. (2007)	**Primary and secondary neurite length** normalized to surface area of cultures with different PLG channel widths were compared. Besides, the former was compared with varying NGF concentration for a given PLG channel width.	[5]
Gertler et al. (2008)	Anatomical differences between D1 MSNs and D2 MSNs were measured by dendritic length, Sholl's analysis, and **number of primary neurites**, critical points, dendrite segments and 3D convex hull analysis (dendritic area).	[6]
Dall'Oglio et al. (2008)	**Number of dendritic branches in each arborization level**, number of branching points, Sholl's analysis and predominant spatial distribution of branches were analyzed for neurons of male and female rats, respectively.	[7]
Henderson et al. (2010)	For examination of effect of shRNA-FRMD7, percentage of cells with neurites, cell with neurite branching, average number of neurite and **average primary neurite length** were compared between undifferentiated and differentiated NEURO2A cells.	[8]
O'Dell et al. (2012)	**Primary neurite length**, total neurite arbor length, numbers of neurites of different order and Sholl's profile were analyzed for wild-type, Reelin-deficient or Reelin-conditioned neuron cultures.	[9]

However, most of the studies utilizing neurite structure employ manual or semi-automatic analysis. Adoption of automatic extraction and quantification of neurite structure will save great amount of time and labor.

1.2.2 Computer-Aided Methods for 2D Neuron Image Analysis

It is labor-intensive and time-consuming to analyze even a single neuron for its neuronal morphologies. Manual analysis of large-database is therefore impractical and user bias is inevitable due to the long-term analysis procedure. As a consequence, development of computer-aided neuronal neuron image quantification method is indispensable. Recently, many computer-aided neuronal morphology extraction and/or quantification tools have been developed (Table 2).

Table 2 Computer-aided studies for 2D neuron images.

Publication		Software Enviromnent			Quantification Task				
Tool Name	Author	Mode	Open-source	Platform	Soma	Neurite	Critical Point	Segment	
NeuronJ	Meijering et al.	S	No	ImageJ	x	LNMSI	x	x	[10]
NeuronStudio	Wearne et al.	S	No	Win	x	LNT	x	x	[11]
NeuronMetric	Narro et al.	S	Yes	ImageJ	x	L	N	x	[12]
HCA-Vision	Vallotton et al.	A	Commercial	Win	NAMPI	LNAMSI	NM	NM	[13]
NeuriteTracer	Pool et al.	A	Yes	ImageJ	NAMPI	L	x	x	[14]
NeuronIQ	Cheng	A	Yes	Matlab	x	L	x	x	[15]
N/A	Leandro et al.	A	No	Matlab	x	x	x	x	[16]
NeuronCyto	Yu et al.	A	Yes	Matlab	NAS	LNM	NM	x	[17]
N/A	Wu et al.	A	Request	Matlab	NAM	LNM	x	x	[18]
NeurphologyJ	Ho et al.	A	Yes	ImageJ	NAM	LAM	NM	x	[19]
NeuriteQuant	Dehmelt et al.	A	Yes	ImageJ	NAM	LAM	NM	x	[20]
WIS-NeuroMath	Rishal et al.	A	Yes	Matlab	NAMI	LAMI	N	x	[21]
NEMO	Billeci et al.	S	Yes	Matlab	NA	L	x	x	[22]
Neurient	Mitchel et al.	A	Yes	Matlab	x	O	x	x	[23]
NeurphologyS		**A**	**Yes**	Matlab	API	LNAMSI	NM	LNMI	

Mode: S, semi-automated; A, automated.

Quantification: N, number; A, area; L, length; M, mean number; I, intensity information.

Soma: P, perimeter; S, shape. Neurite: T, tree level order; S, neurite structure; O, orientation.

For example, NeuronJ [10] provides a semi-automated and accurate neurite labeling GUI, given a pair of starting point and ending point, it can extract an optimal path with globally minimal cost under a predefined cost function; NeuronStudio [11] achieves automated 3D detection and shape classification of dendrite spine, but semi-automatic neurite tracing of 2D neuron image is also provided; NeuronMetrics [12] estimates fundamental information about size and shape of neurite arbors, but it's

semi-automatic and require some extent of manual intervention; the commercial software HCA-Vision [13] is an automatic neurite branching detection and analysis system that is fast, sensitive and reliable; NeuriteTracer [14] analyzes fluorescent microscopy images of neurites and nuclei, traces neurite and measures the neurite length; NeuronIQ [15] aims to provide an automated pipeline for quantitative, reproducible and accurate detection and analysis of neuron dendritic spines; [16] automatically exacts contour from 2D neuron images, however, source code and quantification result are not available; NeuronCyto [17] presents a fully automatic solution for neurite length measurement and complexity analysis; [18] presents a robust method for quantifying and statistically analyzing the morphology of neuron cells in high content screening images; NeurphologyJ [19] can automatically extract five neuronal morphology descriptors from neuron images with a set of user-defined parameters; NeuriteQuant [20] provides a framework for morphometric analysis of neuronal development, including readily adaptable feature extraction and web-based data management; WIS-NeuroMath [21] is a software package for automated measurement of neuronal process, including neurite growth, branching, regeneration or degeneration under different experimental paradigms; Neuritent [22] provides unsupervised method with tunable parameters for neurite extraction; NEMO [23] is developed to handle massive images for automatic batch process and applying multivariate classification and feature extraction.

As Table 2 shows, there are few studies that can automatically analyze neurite structure. However, HCA-Vision, one of these outstanding studies, despite its performance and user-friendliness, is a commercial software. Therefore, in this study, we aim at developing NeurphologyS, an automatic system to extract and quantify neuronal morphological features including neurite structure descriptors. Because of the complexity of neurite outgrowth, automated analysis of neurite structure from

images of densely cultured neurons is impractical with existence of overlapping neurites. The proposed system is tailored toward sparsely stained neuron population.

For extraction of neurite structure, branch order decision is a necessary task. NeurphologyS achieves branch order decision with the proposed RANBO method. Given a sparsely stained neuron image and a set of user-defined parameters, we will automatically extract and quantify 53 neuronal morphological features that perform well compared to HCA-Vision. Owing to its fully-automated property, NeurphologyS eliminates possible discrepancies resulted from different human biases or from unreliable human subjective, and high-throughput analysis of large amount of image dataset is possible.

1.3 Organization of the Thesis

The thesis is organized as follows. In Chapter 1, motivation of this work and related applications and methods are mentioned. In Chapter 2, we describe the datasets used and the proposed system, including basic neuronal morphologies detection, the proposed RANBO method, morphological feature quantification and graphical user interface (GUI). In Chapter 3, experimental results are given to compare the performance of the proposed system with that of existing commercial software. Finally, in Chapter 4, brief conclusion and future works are discussed.

1.4 Participants

The GFP hippocampal neuron images used for developing the proposed system are provided by Dr. Eric Huang's laboratory. And the hippocampal neurons were cultured, imaged and manually annotated by research assistant Wen-Shin Chen. Thanks to her work on neuron image acquisition and neurite structure annotation.

CHAPTER 2

PROPOSED SYSTEM

In this chapter, we will describe the neuron image datasets used in this thesis, and then the proposed system for automatic extraction and quantification of neuronal morphological features. As Fig. 2 shows, the system includes basic neuronal morphologies detection, the proposed RANBO method for neurite branch order decision and quantification of all detected morphological features. Finally, we describe how to utilize the proposed system with the GUI.

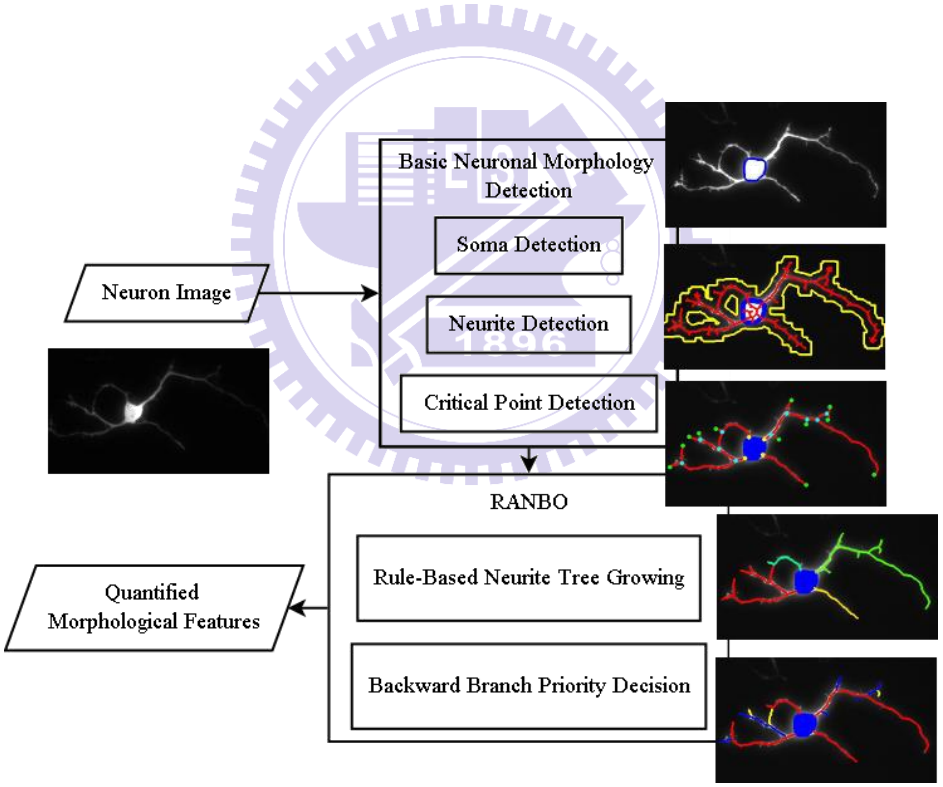

Fig. 2 Block diagram of NeurphologyS.

2.1 Neuron Image Dataset

Two neuron image datasets are used in this thesis, one is image dataset of green fluorescent protein (GFP) transfected hippocampal neurons, the other is the seizure-related gene 6 (Sez-6) knockout cortical neuron image dataset available on the website of HCA-Vision [13].

2.1.1 GFP Transfected Hippocampal Neuron Image

Of the GFP transfected dataset, embryonic hippocampal neuron cells were cultured and transfected with shRNA and GFP expressing plasmid by liposome. Since only up to 25% of the neuron cells can be successfully transfected with GFP, we can acquire images of neuron cells that were not in contact with other cells from the sparsely GFP expressing neuron population.

Forty GFP neuron images, including 41 target neuron cells, were collected as a dataset for the development of NeurphologyS. The dataset can be divided into two subsets according to the complexity of neurite structure of the target neuron. The one without neurite crossovers consists of 23 images (Fig. 3 (a), (b)), and the other with neurite crossovers consists of 17 images (Fig. 3 (c), (d)). Neurite structure of all the target neurons was annotated by a neuroscientist with NeuronJ [24].

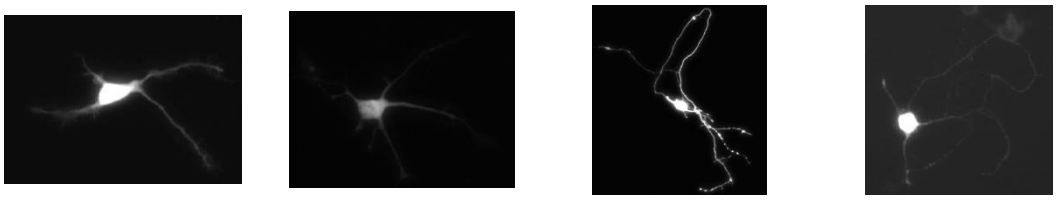

(a) (b) (c) (d)

Fig. 3 Cropped example images of the GFP dataset.

(a) and (b) are neurons without neurite crossovers, (c) and (d) are neurons with neurite crossovers.

2.1.2 Sez-6 Knockout and Wild-type Cortical Neuron Image

Seizure-related gene 6 (Sez-6) is required for normal dendrite arborizaiton, lack of Sez-6 will cause excessive neurite branching [25]. The Sez-6 knockout and wild-type cortical neuron cells were cultured in low density and imaged by HCA-Vision [13]. Fifty images were acquired for wild-type neuron population (Pos) and 46 images were acquired for Sez-6 knockout neuron population (Min). Of the 96 neuron images, 101 image fields of cortical neurons were analyzed (Fig. 4).

By comparing 51 wild-type neurons with 50 Sez-6 knockout neurons, they derived statistical differences in several morphological features of the two types, in agreement with semi-automated analysis results. The image dataset, quantification results accompanied with result images overlaid with automated neurite structure annotation are all available on the website of HCA-Vision.

Table 3 Image and Neuron Amount of Sez-6 Dataset.

	Wild-type (Pos)	Sez-6 Knockout (Min)	Total
Image Number	50	46	96
Neuron Number	51	50	101

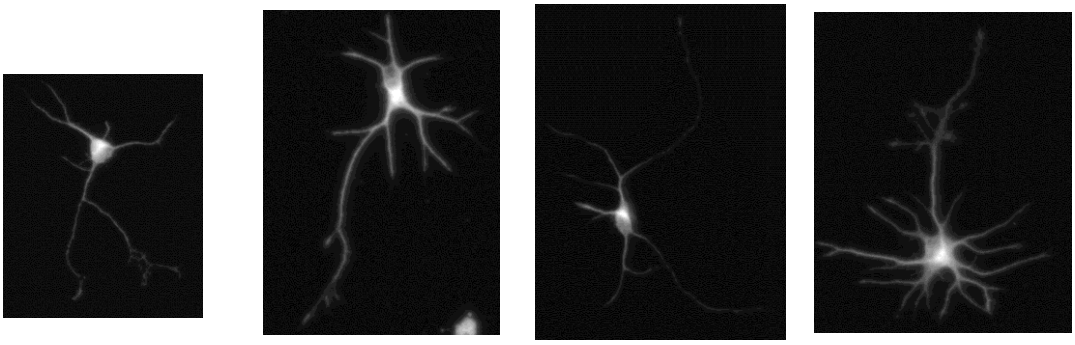

(a) (b) (c) (d)

Fig. 4 Cropped example images of the Sez-6 dataset.

(a) and (b) are wild-type neurons, (c) and (d) are Sez-6 knockout neurons.

2.2 Basic Neuronal Morphology Detection

In this section, we will detect several basic neuronal morphologies from the neuron images. The basic neuronal morphologies include soma (the neuron cell body), neurite and critical points (attachment points, endpoints and branch points).

2.2.1 Soma Detection

At first, we will segment soma region out from neuron images. Due to individual differences of neuron cells, the ability of each neuron to express fluorescence varies (Fig. 5). As a consequence, it is hard to use only one global threshold to segment the soma region even for neurons in the same image dataset.

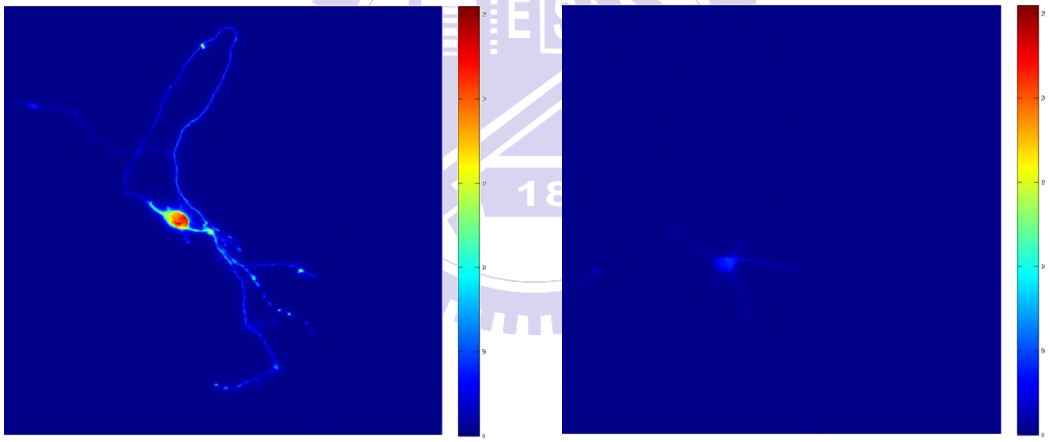

(a) (b)

Fig. 5 Variance of fluorescence expression.

Red and blue represents maximal and minimal brightness, respectively. (a) A neuron with strong fluorescence expression. (b) A neuron with weak fluorescence expression.

In help of manual soma threshold selection, we adopt histogram modification based method [26] as HCA-Vision [13, 27, 28]. The block diagram of soma detection is depicted in Fig. 6.

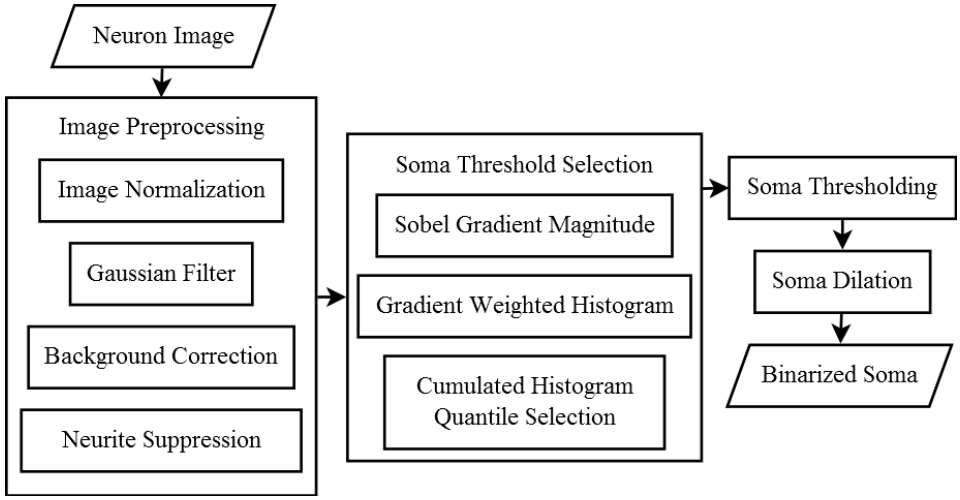

Fig. 6 Block diagram of soma detection.

At the beginning, we linearly stretch the dynamic range of the neuron image to [0, 65535] as the function below:

$$I_{new} = \frac{I - I_{min}}{I_{max} - I_{min}} \times 65535,$$

where I is the original intensity value, I_{max} and I_{min} are the maximal and minimal intensity of the original image and I_{new} is the normalized intensity value.

After, a Gaussian filter is applied for noise suppression. And then we correct the background intensity by morphological top-hat transform [29] with a disk structural element larger than the largest soma. Eventually, to suppress influence of the neurite-like structures, morphological open operation is applied (Fig. 7).

(a) (b)

Fig. 7 Image preprocessing intermediate result of soma detection.

(a) Original image. (b) Preprocessed image, neurite-like structures are eliminated.

With the preprocessed image, we employ histogram modification based method [26] to help soma threshold selection [13, 27, 28]. We expect the region of foreground (soma) and background to have slight intensity change. Hence a gradient filter can get high responses only in background-foreground transient pixels (Fig. 8 (a)). The adequate threshold for foreground segmentation will possibly locate at these pixels. This property is utilized to suppress foreground and background pixels.

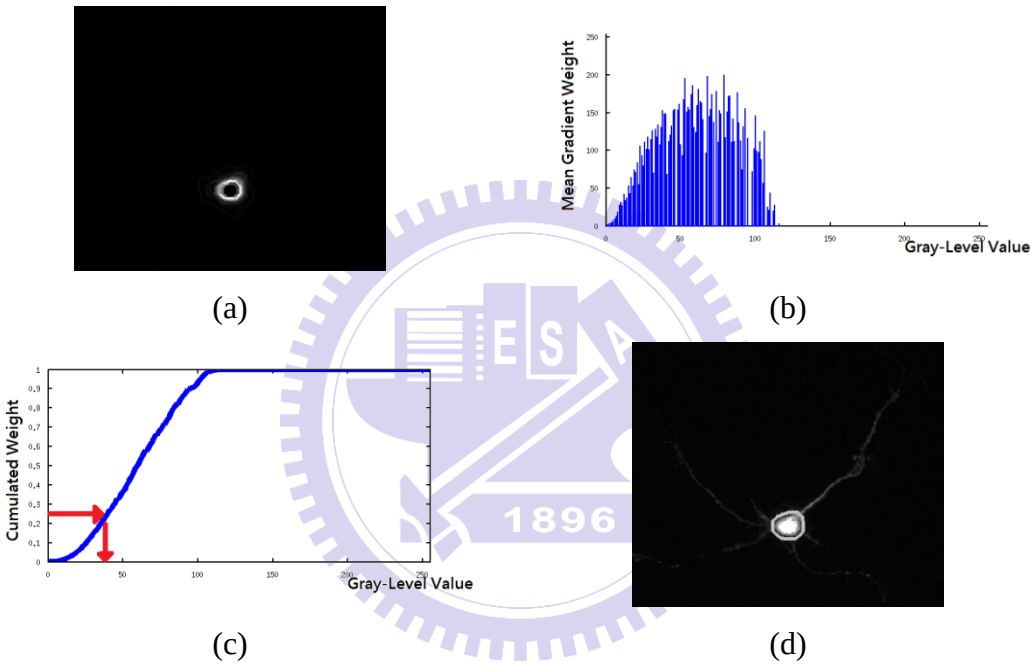

Fig. 8 Histogram modification method for threshold selection.

Follow the example of Fig. 7. (a) Sobel gradient magnitude. (b) Gradient weighted histogram. (c) Cumulated histogram for threshold selection. (d) Segmented soma region.

Firstly, we calculate the gradient magnitude of Sobel filter (Fig. 8 (a)). The gradient magnitudes of the pixels with the same gray-level value are averaged. All these averaged gradient magnitudes can compose a one-dimensional array, referred to as gradient weighted histogram (Fig. 8 (b)). And the cumulated histogram of the gradient weighted histogram is calculated (Fig. 8 (c)).

As described above, owing to the suppression of foreground and background, transient intensities will account for most of the cumulated histogram. Manual selection of quantile will result in different thresholds for different images (Fig. 8 (d)). In addition, the soma is dilated for avoiding the missing of primary neurite. The neurons possess different expression ability as shown in Fig. 5 can now be segmented with the same manually selected cumulated histogram quantile (Fig. 9).

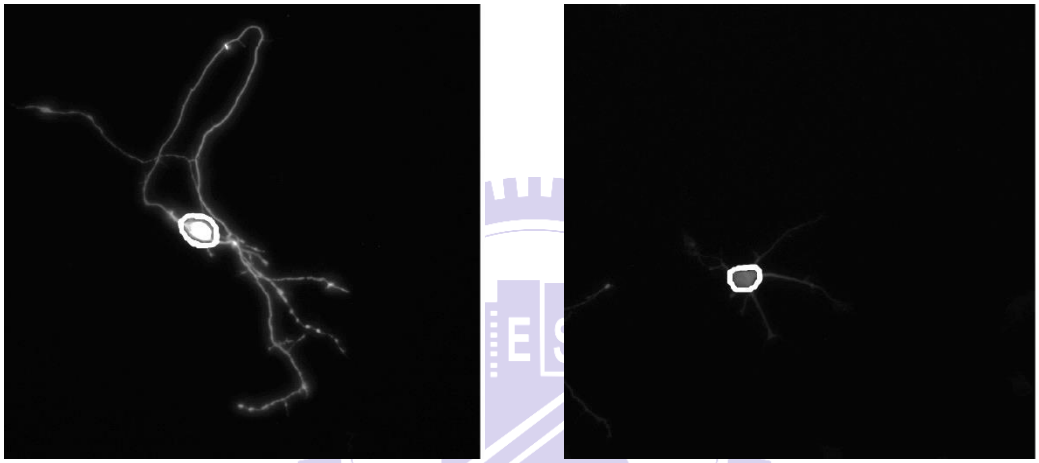

(a) (b)

Fig. 9 Example soma detection results.

Soma detection with histogram modification corresponding to Fig. 5.

2.2.2 Neurite Detection

At first, image processing is applied as described in soma detection step, but eliminating the neurite suppressing morphological open operation. The instability of intensity along neurite in neuron image (Fig. 10) makes it more difficult to segment neurite than segment soma. Hence, multiple directional non-maximal suppression (MDNMS) [13, 30] is employed to extract neurite centerline.

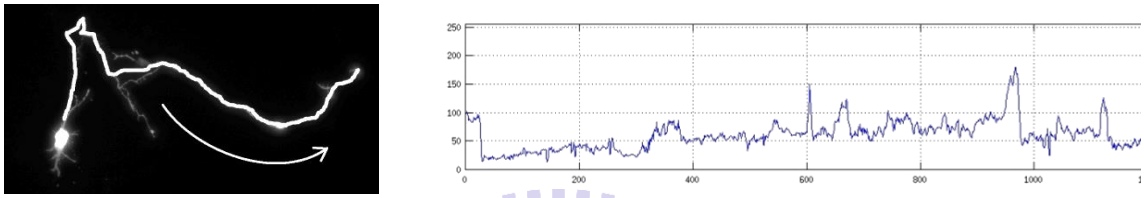

(a) (b)

Fig. 10 Variability of neurite intensity.

(a) A neuron image overlaid with a neurite marked in white. (b) Intensity profile along the neurite centerline in (a).

After, we filter small connected component and skeletonize the MDNMS result to ensure one-pixel wide neurite centerline. Since it is possible that MDNMS fails to detect neurite centerline nearing intersection of neurite, a neurite gap closing step is applied. The overall block diagram is depicted (Fig. 11).

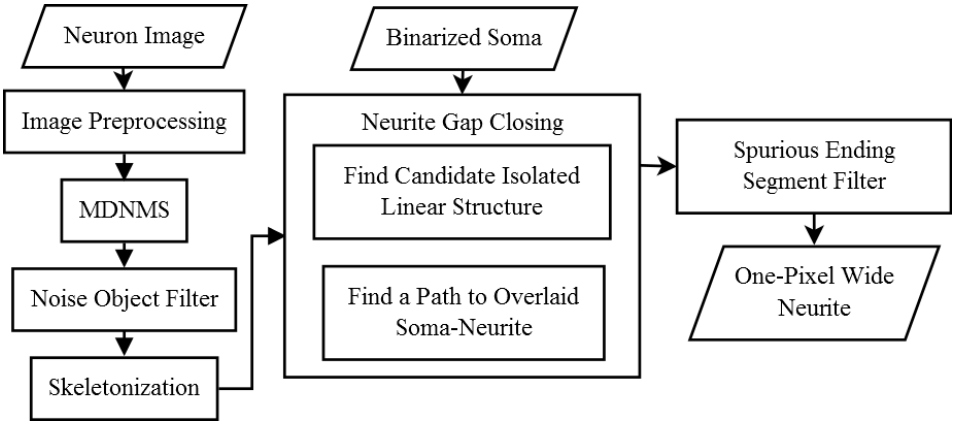

Fig. 11 Block diagram of neurite detection

NMS method is for finding image pixels that locate at intensity cross section maxima within a local liner neighborhood (Fig. 12 (a)). The linear features found perpendicular to the linear window satisfy what we expect neurite centerlines to be (Fig. 12 (b)). Besides, the difference between the local maximal intensity and the averaged intensities of the two-side neighborhoods must exceed a certain extent for maintaining confident high-contrast linear features.

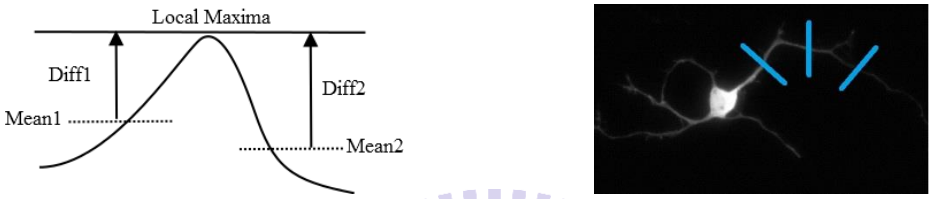

(a) (b)

Fig. 12 Schematic diagram of linear features.

(a) NMS find local maxima with the intensity differences (Diff1 and Diff2) higher than a threshold. (b) Linear windows can detect the neurite centerline.

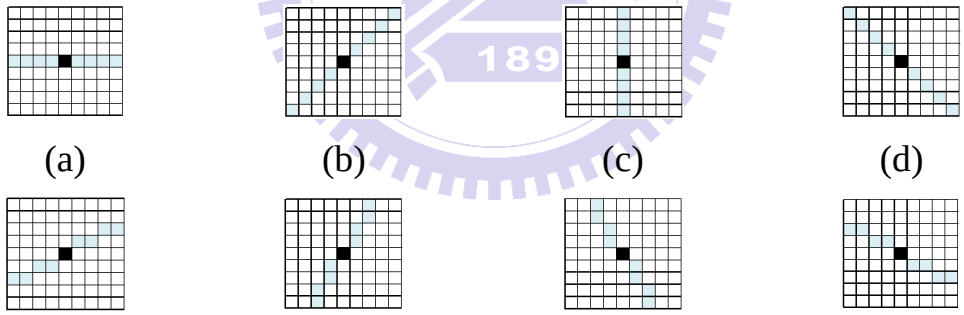

(a) (b) (c) (d)

(e) (f) (g) (h)

Fig. 13 Example 9-by-9 linear windows

Eight directions of linear windows are shown, with dark squares mark centers of each linear window, and gray squares mark the neighborhoods. (a) 0° (b) 45° (c) 90° (d)135° (e)22.5° (f)67.5° (g)112.5° (h)157.5°

Multiple linear windows of different orientations (Fig. 13) can be used in the NMS process. And MDNMS is the union of results of multiple NMS. With MDNMS, pixels where neurite centerlines of different orientations possibly locate can be

detected (Fig. 14 (a)). We then filter smaller connected components of MDNMS result, and apply skeletonization for one-pixel wide skeleton (Fig. 14 (b)).

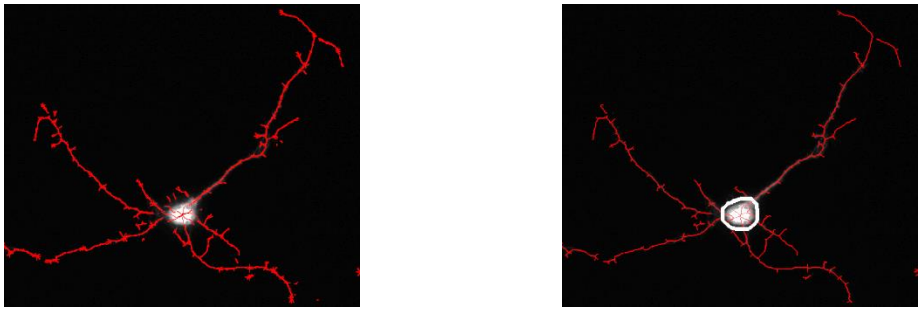

(a) (b)

Fig. 14 Neurite centerline detection with MDNMS.

Follow the example of Fig. 8. (a) MDNMS result. (b) Result after filtering of small connected components and skeletonization, the soma is encircled white.

To fix the possible disconnection of neurites from MDNMS result, at first, we find the neurites overlaid with soma, since only the neurites connected to soma are under consideration. And then we explore the neighborhood of the overlaid neurites as well as soma for finding neighboring isolated connected components (Fig. 15 (a)). The connected components with too small radius or brightness are ignored.

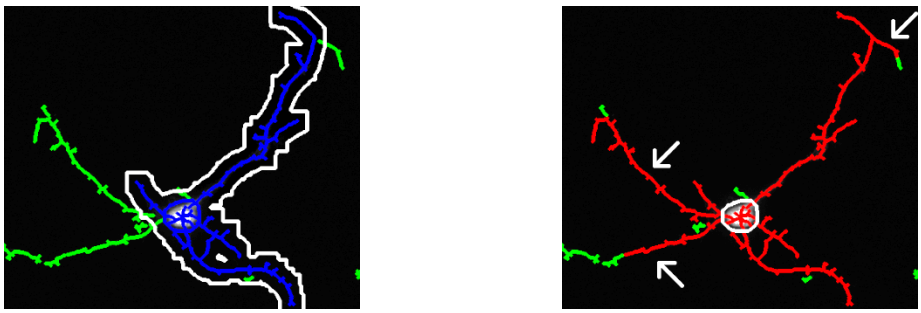

(a) (b)

Fig. 15 Neurite gap closing.

(a) Overlaid region are marked in blue. The region encircled white is the extended region. Isolated linear features are in green. (b) The arrows indicate the added components.

For each of the candidate connected components, we want to find a path of high intensity from its endpoint to a nearest neurite-soma overlaid pixel. The intensity of each current possible direction is considered, the higher the intensity, the lower the cost. Besides, the local orientation of the connected components is used to limit the possible directions of path finding. The positions located at orthogonal or reversed direction of the local orientation are rejected. The path found is added to the skeleton and the candidate connected component is now connected with soma (Fig. 15 (b)). Eventually, we preserve only the skeleton overlapped with soma.

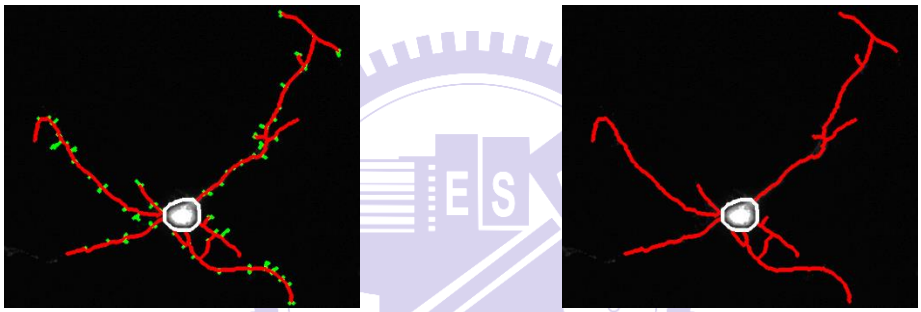

(a) (b)

Fig. 16 Ending segment filtering.

(a) Neurites are in red, and eliminated segments are in green. (b) Result neurite.

The neurite skeleton might contain ignorable spurious linear features, including the linear features inside neuron cell and short ending neurite segments. Ending segment means the segment from endpoints to a nearest branch point or attachment point. Detection of these critical points will be described in the next subsection. For filtering short ending segments, we repeatedly remove the short ending segments until there doesn't exist any short ending segments (Fig. 16).

2.2.3 Critical Point Detection

Critical points (Fig. 17) here include 1) attachment points, pixels where neurite originates from soma 2) endpoints, pixels located at the terminal positions of neurite 3) branch points, pixels where the one-pixel wide neurite bifurcates into two branches.

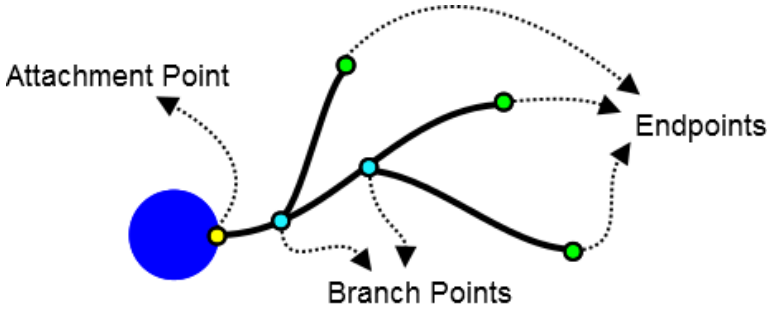

Fig. 17 Schematic diagram of critical points.

The neurite pixels next to the soma perimeter are marked attachment points. And the terminal points of neurite except for attachment points are marked as endpoints.

For branch point detection, since the neurite is skeletonized, the bifurcations of the centerline can be identified in each 3-by-3 local region. Hence we design 16 pairs of 3-by-3 masks (Fig. 18 (a)) representing possible branching patterns. Employing hit-or-miss transform [29] with these masks, we find 50 possible branching patterns (Fig. 18 (c)). As the method mentioned in [31], each 3-by-3 branching pattern can be uniquely represented by a convolution value after convolving the neurite image with a special 3-by-3 mask (Fig. 18 (b)). Therefore, we can fast locate branch points by finding their corresponding convolution value. An example result of critical points detection is shown (Fig. 19).

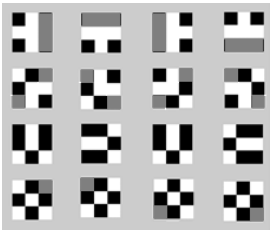

(a)

1	2	4
128	256	8
64	32	16

(b)

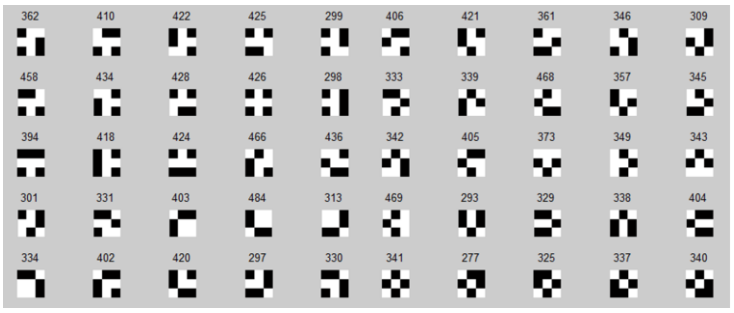

(c)

Fig. 18 Brach point pattern detection.

(a) The 16 3x3 masks used by hit-or-miss transform, white represents foreground pixel, black represents background pixel and grey represents don't care pixel. (b) The 3x3 convolution mask. (c) Branch patterns found by hit-or-miss transform accompanied with their convolution numbers.

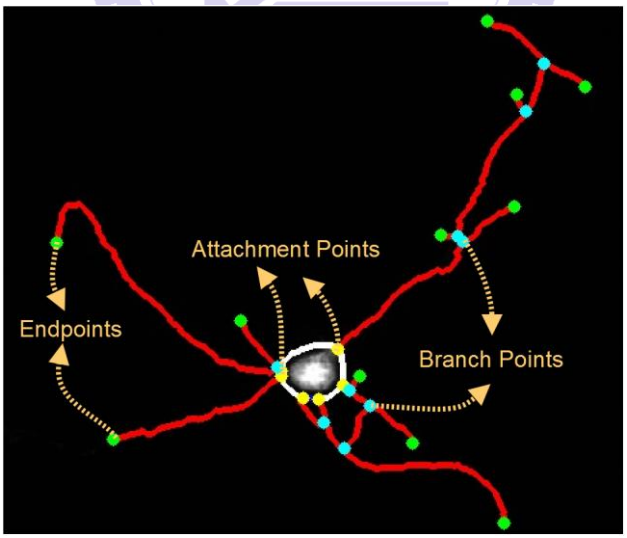

Fig. 19 Result of critical point detection.

The critical points are colored as described Fig. 17.

2.3 Rule-based Neurite Tree Growing and Backward Brach Priority Decision (RANBO)

In this section, we will extract neurite structure based on previously detected basic neuronal morphologies. As described before, neurite structure includes neurites of different branch orders. Neurites of low branch order, of high branch priority in other words, are considered as the backbone of the neurite tree originated from it.

Hence, heuristically, we would expect a lower-order neurite possesses longer length, smoother curve, wider width, stronger fluorescent expression and greater amount of branches compared to higher-order neurites. HCA-Vision employed only the stronger fluorescent expression heuristic within its process of neurite branch priority decision.

To better mimic the human annotation behavior, the proposed RANBO method is established on more than one of these heuristics. Out of the heuristics, the concept of curve smoothness is adopted in the rule-based neurite tree growing step. On the other hand, the concepts of longer length as well as number of branches are adopted in the backward branch priority decision step.

2.3.1 Rule-based Neurite Tree Growing

With neuronal morphology represented neurons (Fig. 20 (a)), we will construct tree-representation of neurite. Each attachment point will be taken as root of the neurite tree originating from it, namely, the attachment points are starting points of depth-first search (DFS). Hence, all the neurite pixels will be assigned to a specific attachment point. Separated with critical points, detected neurites can be further divided into neurite segments. In our tree-representation, the internal nodes are the neurite segments ending with a branch point, and the leaf nodes are the neurite

segments ending with an endpoint (Fig. 20 (b)).

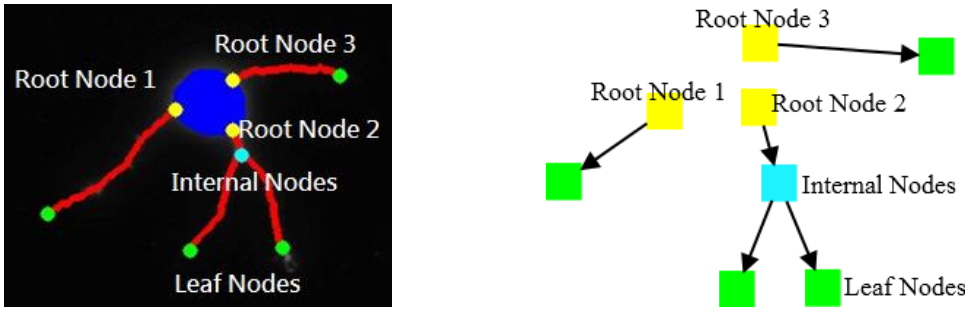

(a) (b)

Fig. 20 Schematic diagram of tree representation.

(a) A neuronal morphology represented neuron. (b) Tree representation corresponding to (a).

However, a tree can be constructed without difficulty only when the neurite anatomy is simple, in other words, when there doesn't exist any neurite crossovers or loops (Fig. 21). Because of the complex neurite growth, we have to decide in each internal node whether this is a bifurcation or a crossover. Complex neurite anatomy will seriously affect the correctness of the constructed tree.

(a) (b)

Fig. 21 An example of neurite crossover.

The region enclosed by white circle is considered a neurite crossover. (a) A neuronal morphology represented neuron. (b) A tree representation separates neurites correctly, separated trees are differently colored.

Hence we will try to employ a local angle related rule set, including empirical rules and bifurcation conditions, to solve this problem. In situations judged as crossovers by the rule set, at least one child segment will be recorded as failed segments. After the current DFS is finished, as long as there are still unvisited failed segments, we continue to add them back one by one as DFS starting points from the one with the minimal angle with its parent segment. The overall flowchart of rule-based neurite tree growing, a DFS combined with rule set applying and crossover handling, is depicted below (Fig. 22).

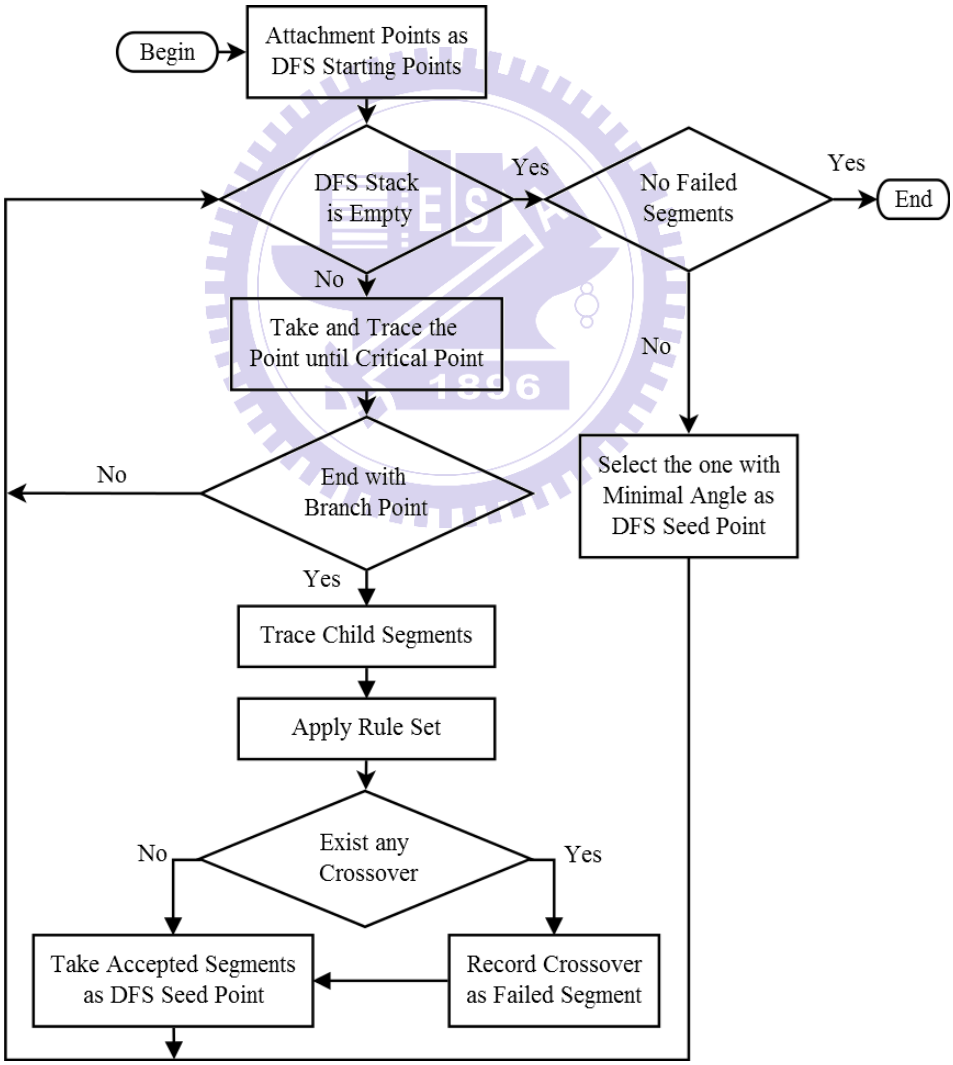

Fig. 22 Flowchart of rule-based neurite tree growing.

To ensure correct tree hierarchy, we will exam several empirical rules concerning the local angle between neurite segments in the DFS process. These rules mimic the human behavior that selects a smooth neurite as the backbone of neurite tree, and what a neurite crossover might look like.

We generalize the situation nearing branch points as Fig. 23. There will be a parent segment P and two branched child segments C_1 and C_2, where the three segments are internal nodes or leaf nodes in our tree representation. Here we define three local angles, the angle between C_1 and C_2 as A, the angles between extended line of P and C_1 are A_1 and the angles between extended line of P and C_2 are A_2.

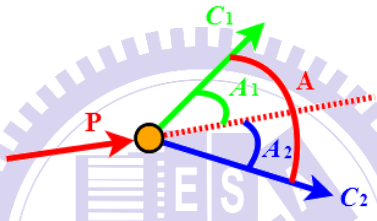

Fig. 23 Situation nearing a branch point.

Parent segment P and Child segments C_1 and C_2 are colored differently. The dashed line represents extension of P. And the branch point is marked by point. Three angles are defined here: A is the angle between the two children; A_1 and A_2 are angles between the extended line and the two child segments, respectively.

From observations, four major rules concerning local segment angle are empirically concluded in Table 4, where the bifurcation angle upper bound α_1, lower bound α_2 and angle ratio threshold β are parameters defined by user. The angle ratios are defined as $\beta_1 = \frac{A_1}{A}$ and $\beta_2 = \frac{A_2}{A}$ for C_1 and C_2 respectively. Since we prefer a smoother neurite curve, when the situation is a bifurcation, the child segment with smaller angle with parent segment will possess higher priority in DFS trace than the other.

Table 4 Local Angle Empirical Rules.

Rules	Content	Result
Rule 1	When $A > \alpha_1$, the C_1 and C_2 seem to comprise another neurite together; we consider this situation a crossover and stop the trace (Fig. 24 (a)).	P is a crossover.
Rule 2	When $A < \alpha_2$, that any combination of angle degree of A_2 and A_3 seems reasonable, this situation is considered a bifurcation (Fig. 24 (b)).	Bifurcation.
Rule 3	When $\alpha_1 \geq A \geq \alpha_2$, if $\beta_1 < \beta$, we prefer C_1 over C_2 (Fig. 24 (c)).	C_1 is a crossover.
Rule 4	When $\alpha_1 \geq A \geq \alpha_2$, if $\beta_2 < \beta$, we prefer C_2 over C_1 (Fig. 24 (d)).	C_2 is a crossover.
Otherwise	The situation otherwise is considered a bifurcation.	Bifurcation.

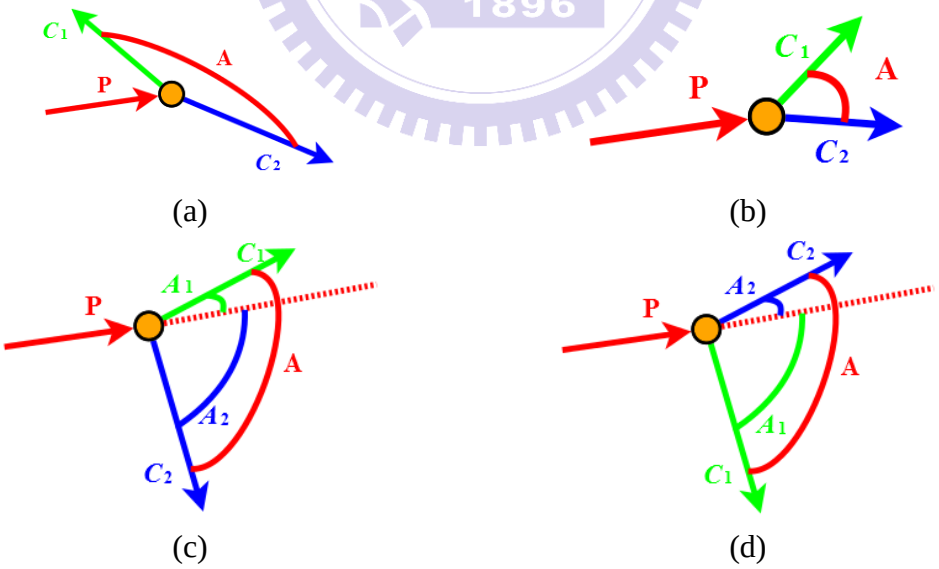

Fig. 24 Schematic diagrams of empirical rules.

(a) A is too large to form a bifurcation. (b) A bifurcation situation. (c)(d) One child segment will be taken as crossover depending on the preference ratio.

In addition to the above mentioned empirical rules, we take the conditions in Table 5 as bifurcations, with corresponding schematic diagrams depicted in Fig. 25. These conditions are examined prior to empirical rules. Once any one of them matched in the DFS process, the situation will be regarded as a bifurcation. The empirical rules accompanied with bifurcation conditions work as a rule set for deciding whether the situation is a crossover or a bifurcation.

Table 5 Bifurcation Conditions.

Conditions	Content
Condition 1	When both C_1 and C_2 are leaf nodes, there are no more possible disturbances for tree construction (Fig. 25 (a)).
Condition 2	Both C_1 and C_2 end at the same point (Fig. 25 (b)).
Condition 3	P is too short to calculate effective angles (Fig. 25 (c)).

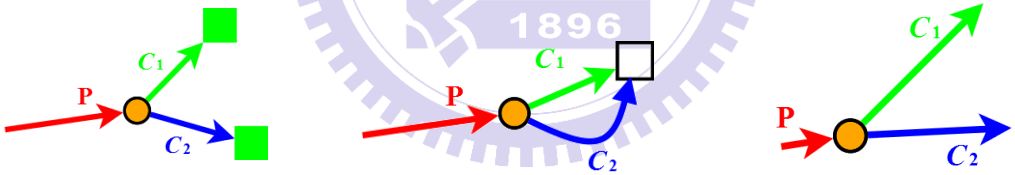

(a) (b) (c)

Fig. 25 Schematic diagrams of bifurcation conditions.

(a) *C1* and *C2* are leaf nodes. (b) *C1* and *C2* end at the same point. (c) *P* is too short.

And then we describe how the rule set works in detail. Firstly, the bifurcation conditions are examined with the order of Condition 1, Condition 2 and Condition 3. Next, the empirical rules are checked from Rule 1 to Rule 4. Once a condition or a rule is matched, examination of the remaining portion of the rule set will be skipped. According to the matched rule, four kinds of decisions can be made: 1) the parent segment p is a crossover 2) the child segment C_2 is a crossover 3) the child segment C_1 is a crossover 4) the situation is a bifurcation. The flowchart of rule set application is depicted (Fig. 26). An example is given to demonstrate the rule-based neurite tree growing method (Fig. 21).

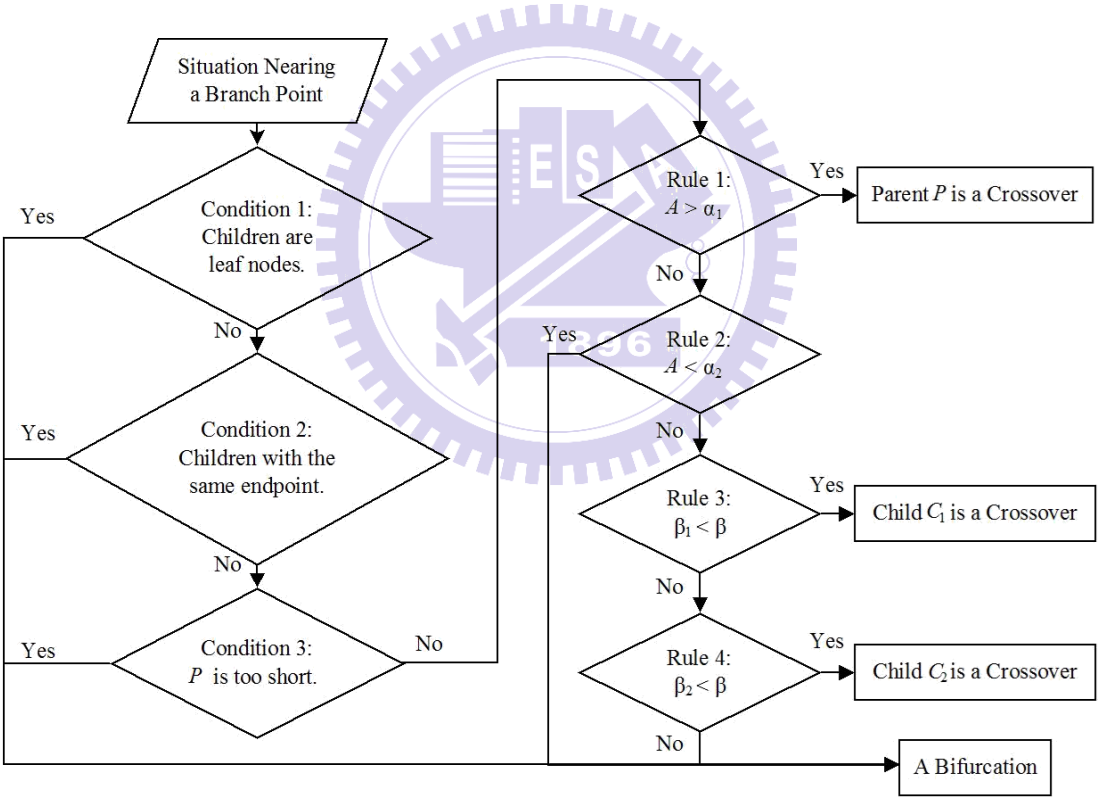

Fig. 26 Flowchart of the rule set application.

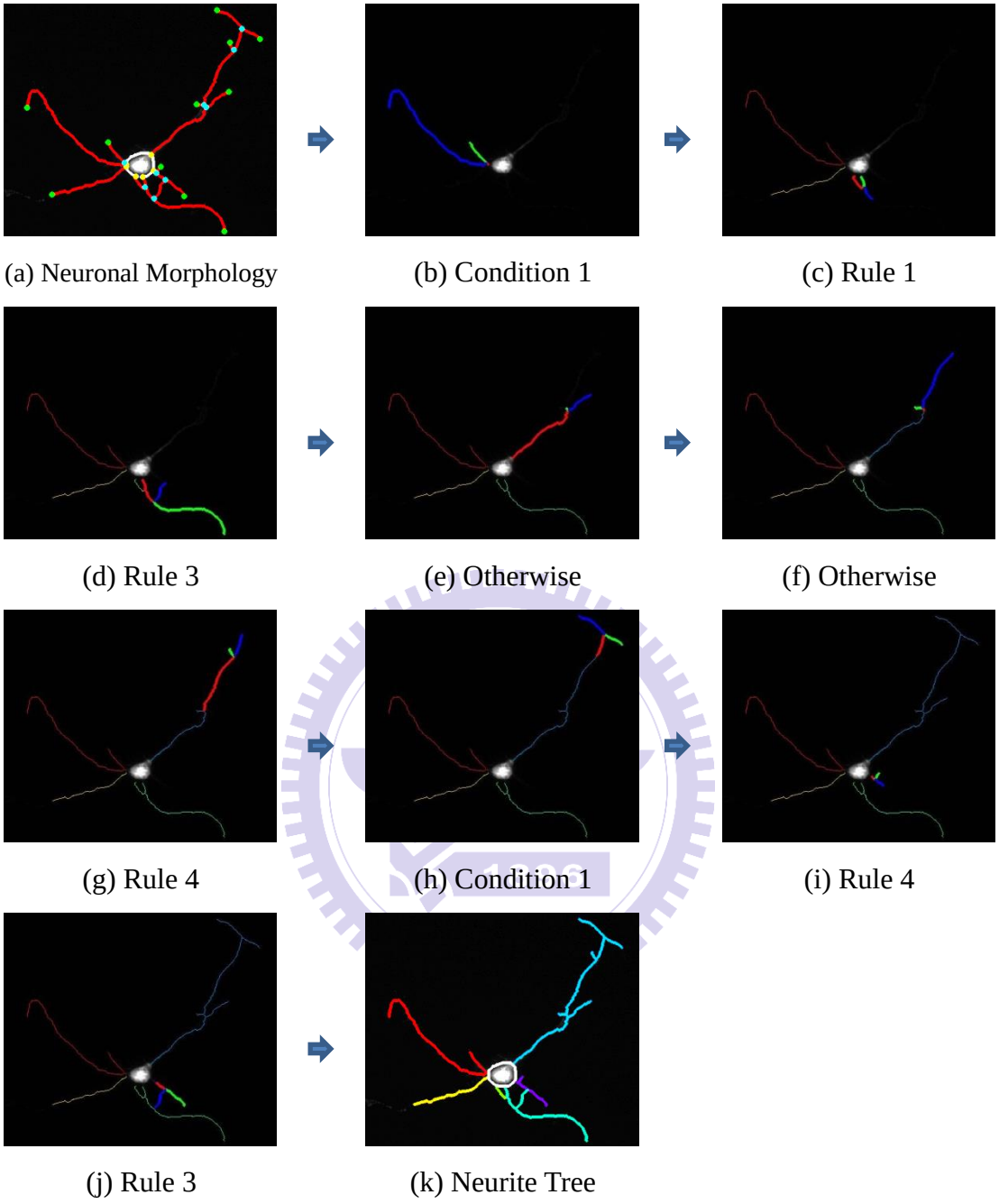

Fig. 27 An example of rule-based neurite tree growing.

(b)~(j) The visited neurite trees are labeled with thin lines of different colors. The bold lines represent the current situation: P (red), C_1 (green) and C_2 (blue).

2.3.2 Backward Branch Priority Decision

With previously constructed neurite trees, in this subsection, we deal with branch order decision. In the neurite tree representation, we can uniquely find all the ancestors of any node until the root node, namely, the paths from an arbitrary attachment point to any branch point or endpoint are unique. However, if we make branch priority decision from the root node, the backbone in the tree originated from the node is unknown. And the power of the information of the subtree is wasted.

Therefore, we employ a backward branch priority decision, in other words, we begin from the leaf nodes and decide branch priority of two subtrees at each bifurcation instead of merely two neurite segments. So, at a bifurcation, only when the two subtrees of the current node are finished can we make priority decision (Fig. 28). The algorithm of backward branch priority decision is described in Algorithm 1. Besides, an example is given (Fig. 29).

Taking the heuristic of longer neurite length and more branches together into consideration, here we adopt total subtree length, which is summed neurite length of all decedent nodes of a node, to decide the branch priority of the two children in the internal nodes.

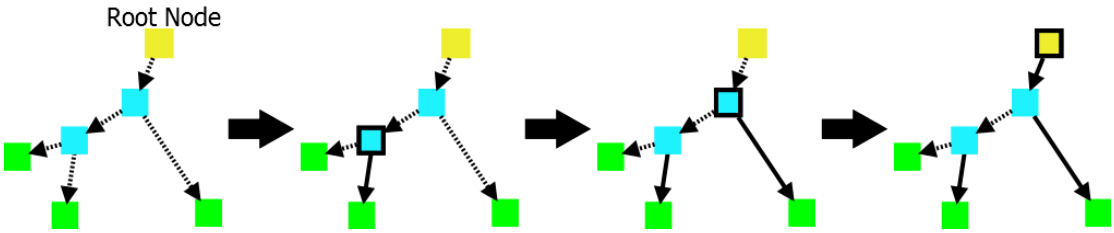

Fig. 28 Schematic diagram of backward branch priority decision.
The square with black frame represents the current node. Dotted line represents segment of low priority and solid line represents segment of high priority.

Algorithm 1 Backward Branch Priority Decision

```
    Input: tree-represented neurite
    Output: neurite tree branch priority
01  Set all internal nodes unvisited.
02  WHILE there exist unvisited nodes, do
03      FOR each unvisited node, do
04          IF the node has unvisited children, then
05              Skip.
06          Collect information for priority decision.
07          Decide priority of the two subtrees.
08          Set the node as visited.
```

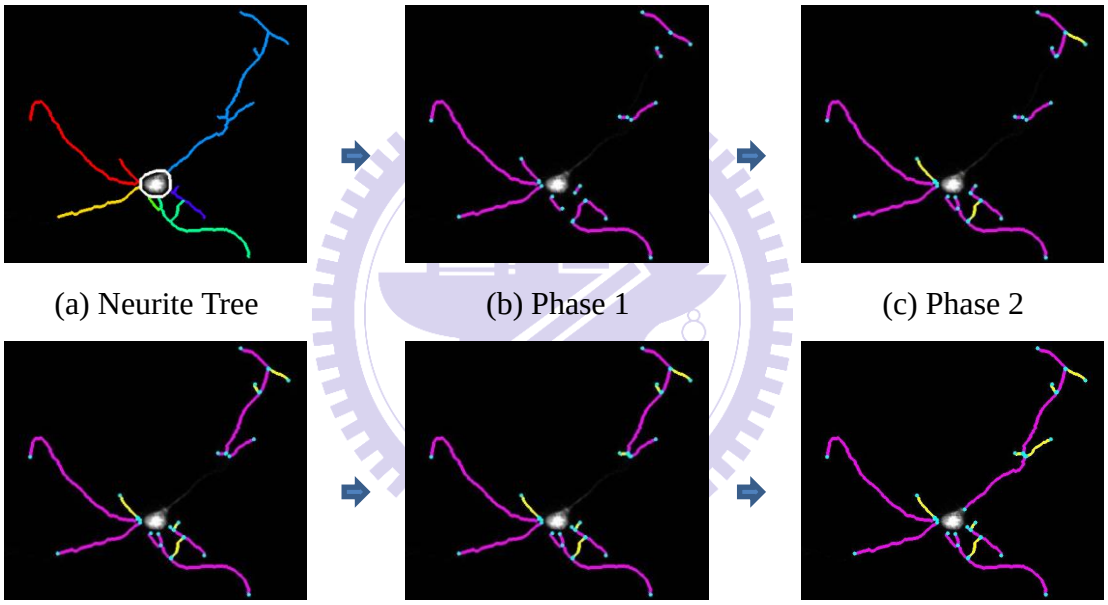

(a) Neurite Tree (b) Phase 1 (c) Phase 2

(d) Phase 3 (e) Phase 4 (f) Branch Priority

Fig. 29 An example of backward neurite branch priority decision.

Follow the example in Fig. 27. In (b) ~ (f), the segments (nodes) with higher priority are marked purple and that with lower priority are marked yellow.

Eventually, after all priority decisions are made, the branch order can be assigned from the root node (Fig. 30), which is undoubtedly part of a primary neurite. For example, of the two child segments of a primary neurite, the one with higher priority will be concatenated with the original primary neurite, and the other will become a new secondary neurite. Similarly, a secondary neurite will elongate at a bifurcation and sprout a tertiary neurite simultaneously.

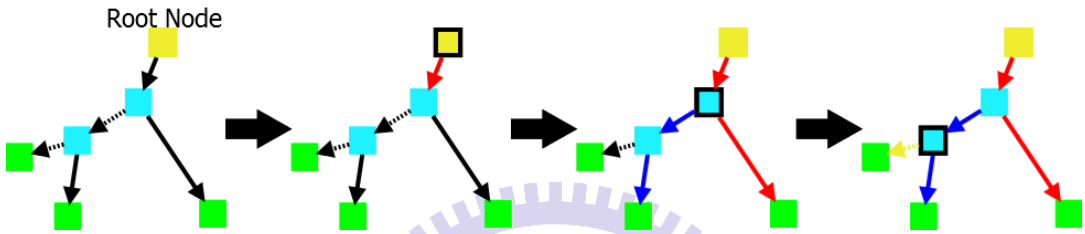

Fig. 30 Schematic diagram of branch order assignment.

Follow from Fig. 28, here red lines represent primary neurites, blue lines represent secondary neurites and yellow lines represent tertiary neurites.

The Algorithm 2 is employed to collect neurites from the neurite tree and simultaneously assign branch order of these neurites. As the example shown (Fig. 31), primary neurites are collected first, and then secondary neurites and so on. After the branch order assignment is done, neurite structure detection is complete and the neurite structure descriptors can be extracted.

Algorithm 2 Neurite Collection with Branch Order

```
   Input: neurite tree with branch priority
   Output: neurites with branch order
01 Collect root nodes of the tree as current stack.
02 Set current branch order as primary.
03 WHILE current stack is not empty, do
04     FOR each node in current stack, do
05         Trace neurite along high priority from the node.
06         Append the neurite to current order neurites.
07     Collect all branches along current order neurites as
       current stack.
08     Add current branch order by one.
```

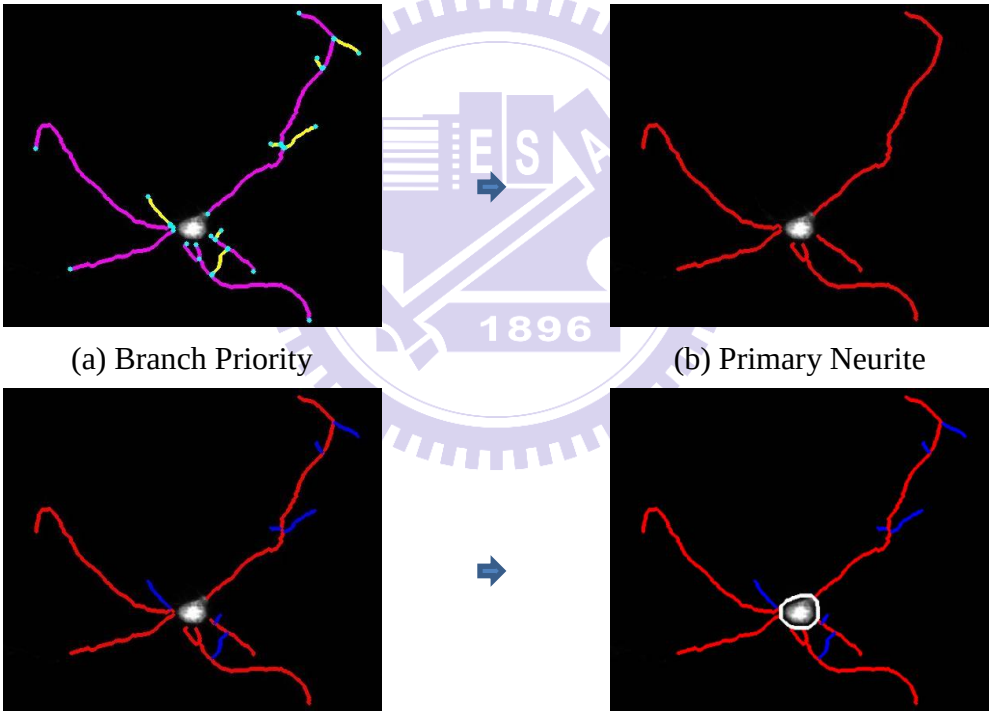

(a) Branch Priority (b) Primary Neurite

(c) Secondary Neurite (d) Branch Order

Fig. 31 An example of neurite branch order assignment.

Follow the example in Fig. 29. In (b) ~ (d), primary neurites are in red and secondary neurites are in blue.

2.4 Quantification of Neuronal Morphological Features

After the extraction of basic neuronal morphologies and neurite structure, we will quantify detected morphological features for each neuron cell. In addition to the neurites, neurite segments, the line segments between critical points, are available for quantification as well (Fig. 32).

(a) (b)

Fig. 32 Schematic diagram of neurites and neurite segments.

(a) A neuron with three neurites marked in different colors. (b) From (a), five neurite segments are separated by critical points.

The 53 quantifiable morphological features for individual neurons of NeurphologyS are summarized (Table 6). Each of these features, according to the subject it describes, can be categorized into five subsets. The subsets accompanied with the number of features are listed:

1) Soma related features (6).
2) Neurite related features (32), including 24 features describing different orders of neurites. Neurites with branch order larger than tertiary are regarded as higher-order neurites.
3) Critical point related features (3).
4) Neurite segment related features (7).
5) Other features that cannot be categorized in the above four subsets (5).

Table 7 describes how to calculate these quantification values. Due to the similarity of calculation, repeated descriptions of quantifications of neurite and neurite segment are eliminated. All the 31 morphological features available in HCA-Vision are included in the feature set of NeurphologyS. Table 8 shows the mapping of morphological features from HCA-Vision to NeurphologyS.

Table 6 Quantifiable Morphological Features of NeurphologyS.

Soma	Primary Neurites	Secondary Neurites
somaArea	primaryNum	secondaryNum
somaPerimeter	primaryLengthMax	secondaryLengthMax
somaIntensityMax	primaryLengthMean	secondaryLengthMean
somaIntensityMean	primaryLengthTotal	secondaryLengthTotal
somaIntensityIntg	primaryBranchNum	secondaryBranchNum
somaIntensityStdv	primaryBranchMean	secondaryBranchMean

Tertiary Neurites	Higher Order Neurites*	All Neurites
tertiaryNum	highorderNum	allNum
tertiaryLengthMax	highorderLengthMax	allLengthMax
tertiaryLengthMean	highorderLengthMean	allLengthMean
tertiaryLengthTotal	highorderLengthTotal	allLengthTotal
tertiaryBranchNum	highorderBranchNum	allIntensityMax
tertiaryBranchMean	highorderBranchMean	allIntensityMean
		allIntensityIntg
		allIntensityStdv

Critical Points	Neurite Segments	Others
endpointNum	segmentNum	branchLayerMax
allBranchNum	segmentLengthMax	branchLayerMean
allBranchMean	segmentLengthMean	subtreeLengthMax
	segmentLengthTotal	subtreeLengthMean
	segmentIntensityMax	neuriteFieldArea
	segmentIntensityhMean	
	segmentIntensityStdv	

Neurite related features (white) are further divided due to the amount.

*Branch order larger than tertiary are regarded as higher order.

Table 7 Morphological Feature Quantification.

Feature Name	Feature Computation
Soma	
somaArea	Total area of the soma.
somaPerimeter	Perimeter of the soma.
somaIntensityMax	Maximum intensity value in the soma.
somaIntensityMean	Averaged intensity value in the soma.
somaIntensityIntg	Summation of intensity values in the soma.
somaIntensityStdv	Standard deviation of intensity values in the soma.
Neurites (Neurite Segments)	
Num	Number of neurites.
LengthMax	Maximum length of neurites.
LengthMean	Averaged length of neurites.
LengthTotal	Summation of lengths of neurites.
BranchNum	Summation of numbers of branches on neurites.
BranchMean	Averaged number of branches on neurites.
IntensityMax	Maximum intensity value in all neurites.
IntensityMean	Averaged intensity value in all neurites.
IntensityIntg	Summation of intensity values in all neurites.
IntensityStdv	Standard deviation of intensity values in all neurites.
Critical Points	
endpointNum	Number of ending neurite segments.
allBranchNum	Number of branches of all neurite trees.
allBranchMean	Number of branches of all neurite trees divided by number of all neurites.
Others	
branchLayerMax	Maximum branch order of all neurite trees.
branchLayerMean	Maximum branch order of all neurite trees divided by the number of primary neurites.
subtreeLengthMax	Maximal total length of neurite trees of different roots.
subtreeLengthMean	Averaged total length of neurite trees of different roots.
neuriteFieldArea	Convex hull area that contains all the neurites.

Table 8 Corresponding Features of NeurphologyS and HCA-Vision.

HCA-Vision	NeurphologyS
Area	somaArea
Perimeter	somaPerimeter
TotalNeuriteLength	allLengthTotal
MaxNeuriteLength	allLengthMax
MaxBranchLayer	branchLayerMax
MeanBranchLayer	branchLayerMean
NumBranchPoints	allBranchNum
NumOfRoots	primaryNum
NumOfSegments	segmentNum
NumOfExtremities	endpointNum
NeuriteFieldArea	neuriteFieldArea
MaxIntensity_Neurite	allIntensityMax
MeanIntensity_Neurite	allIntensityMean
IntegratedIntensity_Neurite	allIntensityIntg
StdevIntensity_Neurite	allIntensityStdv
Lvl1NoBranches	primaryNum
Lvl1TotLength	primaryLengthTotal
Lvl1MaxLength	primaryLengthMax
Lvl2NoBranches	secondaryNum
Lvl2TotLength	secondaryLengthTotal
Lvl2MaxLength	secondaryLengthMax
Lvl3NoBranches	tertiaryNum
Lvl3TotLength	tertiaryLengthTotal
Lvl3MaxLength	tertiaryLengthMax
MaxIntensity_Neuron	somaIntensityMax
MeanIntensity_Neuron	somaIntensityMean
IntegratedIntensity_Neuron	somaIntensityIntg
StdevIntensity_Neuron	somaIntensityStdv
Mean primary length	primaryLengthMean
Mean sec length	secondaryLengthMean
Mean tert length	tertiaryLengthMean

2.5 Quantify Morphological Features with NeurphologyS

NeurphologyS is implemented in MATLAB, hence it is cross-platform. For ease of use, a GUI is provided (Fig. 33). The usage of NeurphologyS GUI is divided into two phases, parameter setting phase and batch processing phase. Here we will describe each parameter in detail. The parameters required by NeurphologyS are separated into two sets, corresponding to basic neuronal morphology detection and the RANBO method. The parameter set of basic neuronal morphology detection is further divided into four parts, for soma detection, neurite detection, neurite gap closing and spur filter. The parameters are summarized in Table 9.

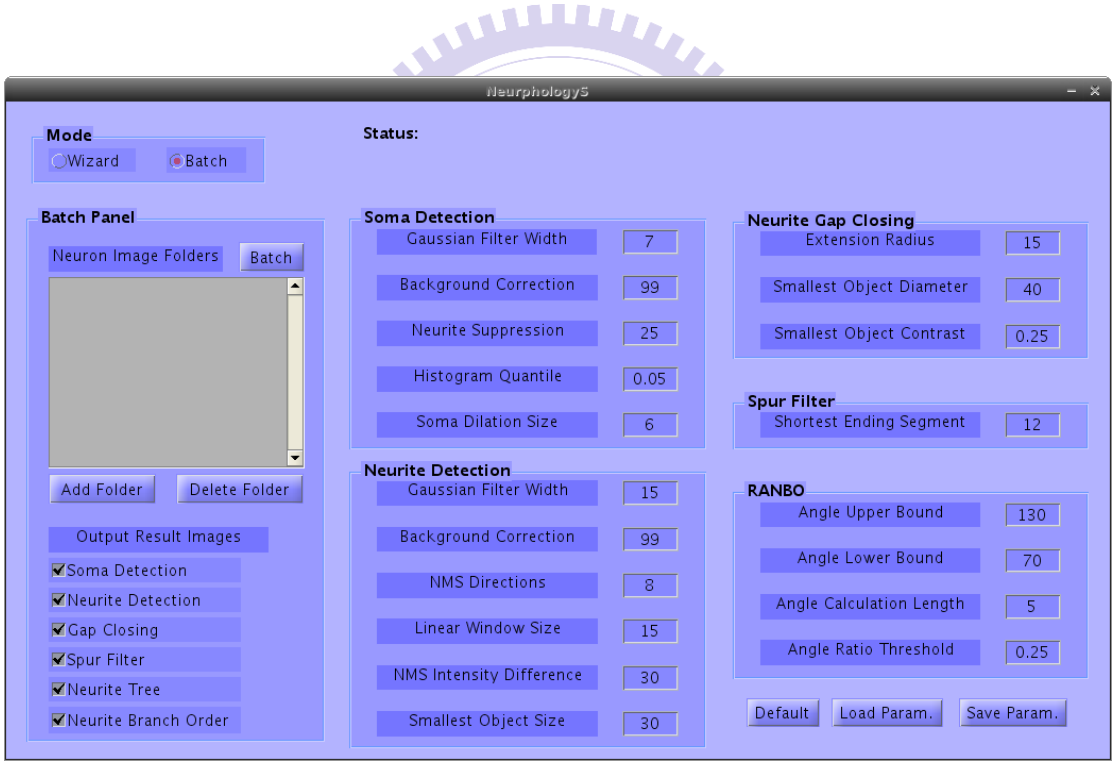

Fig. 33 Graphical user interface of NeurphologyS.

Table 9 Parameters of NeurphologyS.

Basic Neuronal Morphology Detection	
Soma Detection	Neurite Detection
Gaussian filter width	Gaussian filter width
Background correction width	Background correction width
Neurite suppression width	MDNMS directions
Cumulated histogram quantile	Linear window size
Soma dilation size	NMS intensity difference
	Smallest object size
Neurite Gap Closing	**Spur Filter**
Extension radius	Least ending segment length
Object diameter	
Object contrast	
RANBO	
Angle upper bound	
Angle lower bound	
Length for angle calculation	
Angle ratio threshold	

Parameters for soma detection are listed: 1) window width of Gaussian filter, the larger the size, the larger the impact of blurring effect of the filter; 2) structural element width for background correction, the size must be larger than the largest soma, otherwise the soma might be eliminated; 3) structural element width for neurite suppression, the size is expected to be larger than the widest neurite width; 4) quantile of the gradient weighted histogram, the smaller the value, the thresholding becomes less sensitive but more noisy; 5) soma dilation size, since the neurite detected can be disconnected from soma detection, the user can specified a size for enlarging soma.

Parameters for neurite detection are listed: 1) window width of Gaussian filter; 2) structural element width for background correction; 3) number of directions used for local linear windows, 4 directions including 0, 45, 90 and 135 degrees, and 8

directions will add 22.5, 67.5, 112.5 and 157.5 degrees in addition; MDNMS with more linear windows of different directions is expected to extract more complete neurite centerlines; 4) liner window width, the size is expected to be close to widest neurite width for detection of centerline; 5) intensity difference of MDNMS, this value means how much the distance from the maxima to the two sides of ridge, larger value eliminates weak linear features; 6) smallest object size, this value is to eliminate small connected components of linear features.

Parameters for neurite gap closing are listed: 1) extend window radius, how far the candidate isolated linear structures can be located near the overlaid soma-neurite component; 2) object diameter, only the linear structures with diameter larger than this constraint are considered; 3) object contrast, linear structures with low contrast, namely, similar to background, are ignored. As for the spur filtering part, the shortest ending segment size determines the length of the ending segments to be removed. Until here the parameters for basic neuronal morphology are all described.

Parameters for RANBO are listed: 1) local segment angle upper bound, the branch point will be regarded as crossover if the local angle is larger than this upper bound; 2) local segment angle lower bound, the branch point will be consider as a bifurcation if the local angle is smaller than this lower bound; 3) the length of segment to be used to calculate the angles; 4) angle ratio threshold, as mentioned before, the smaller the value, the more strictly that one of the two child branches will be regarded as a crossover.

Given a test neuron image of a dataset, the user can tune parameters with the NeurphologyS wizards (Fig. 34 (a)). The result of parameter adjust of separated steps can be visualized. These parameters can be stored and be used in batch process phase (Fig. 34 (b)). In batch process phase, the user can select folders of neuron images to be processed with the stored parameters. In the end of the process, descriptors are

calculated for each detected soma, and the results are written into the same tab-delimited text file for the images in the same folder. In addition, result images can be saved also for visualization.

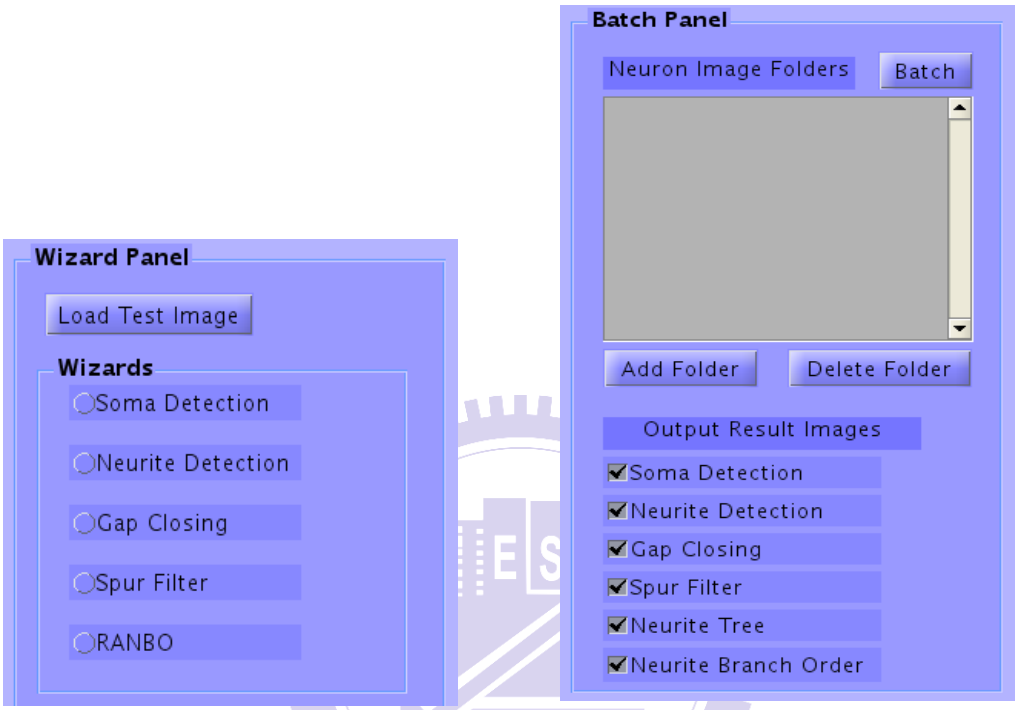

(a) (b)

Fig. 34 Two operation modes supported by the GUI.

(a) Wizard mode, it's for ease of tuning five different parameter sets. (b) Batch processing mode, with a set of parameters, the user can batch process images in selected directories.

CHAPTER 3

EXPERIMENTAL RESULTS

In this chapter we will evaluate performance of NeurphologyS by comparing with the existing commercial software HCA-Vision [13]. Firstly, both our method and HCA-Vision is applied on the GFP image dataset for evaluating the basic neuronal morphology quantifications. Secondly, we process the Sez-6 image dataset for proving the ability to differentiate subtle change in neurite branching. Finally, semi-automated method (NeuronJ [10]) results are taken as ground truth and show that NeurphologyS mimics human behavior well compared to HCA-Vision.

3.1 Comparable Quantification Results with HCA-Vision

To compare the performance of basic neuronal morphology quantification of the proposed system, in this experiment, we process our GFP dataset with both NeurphologyS and HCA-Vision (Fig. 35). The 40 neuron images are processed with the same set of parameters, and 41 neurons are selected for quantification. Although 53 features can be quantified, only the 31 morphological features corresponding to that can be exported by HCA-Vision are shown for comparison.

Table 10 shows the mean value and standard deviation of each features derived using NeurphologyS and HCA-Vision, respectively. In addition, Pearson's correlation coefficients between corresponding features of NeurphologyS and HCA-Vision are calculated. The correlation values are used for ranking in the table to show what are the most correlated features.

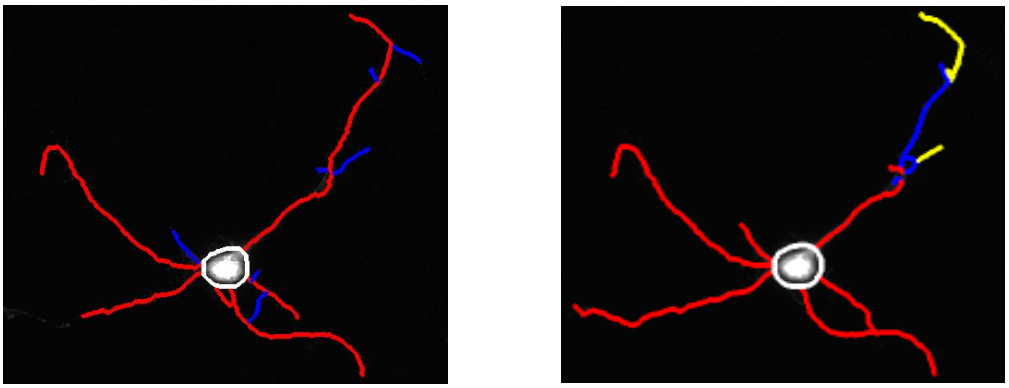

(a) (b)

Fig. 35 Example result image of the two methods on GFP dataset.

(a) Result image of NeurphologyS. (b) Result image of HCA-Vision.

Of the 31 morphological features, 17 descriptors are irrelevant to neurite structure, such as total neurite length, maximal neurite intensity or number of roots. These descriptors will not affected by neurite branch order decision. The remaining 14 descriptors are neurite structure related. It can be observed from Table 10 that the most correlated features are neurite structure irrelevant and that most neurite structure related descriptors are less correlated.

Of the 10 highly correlated features (with correlation value > 0.9), 7 of them are intensity-related features. This shows similarity of the soma detection and neurite centerline extraction of the two methods. The high correlation of total neurite length and neurite field area shows similarity of neurite detection also. Hence, the less correlated neurite structure features might be resulted from the difference of the two method in the composition of neurite branch order.

As a brief conclusion, our detection of basic neuronal morphology is comparable to the validated commercial software. And the following comparisons on neurite structure can be made on this basis.

Table 10 Quantification results of the GFP dataset.

Descriptors	NeurphologyS		HCA-Vision		Correlation
	Mean	STDV	Mean	STDV	
MaxIntensity_Neuron	230.3	48.2	230.1	48.3	**1.00**
IntegratedIntensity_Neuron	277644	107214	266542	105151	**0.99**
IntegratedIntensity_Neurite	22073	24288	29390	33655	**0.99**
StdevIntensity_Neuron	68.5	18.6	64.9	19.3	**0.98**
NeuriteFieldArea	108473	119099	100807	108007	**0.97**
StdevIntensity_Neurite	13.9	8.7	13.4	8.3	**0.96**
MeanIntensity_Neurite	20.0	12.6	21.0	13.3	**0.96**
TotalNeuriteLength	1097.6	855.5	1149.2	804.7	**0.93**
MaxIntensity_Neurite	92.4	54.8	86.6	51.2	**0.92**
Lvl3TotLength	47.6	99.1	147.6	354.7	**0.91**
MaxNeuriteLength	405.5	290.8	476.4	354.1	0.88
MeanIntensity_Neuron	100.0	27.1	110.9	28.4	0.87
NumOfRoots	3.9	1.5	3.9	1.4	0.84
Lvl1NoBranches	3.9	1.5	3.9	1.4	0.84
NumOfExtremities	10.0	6.2	9.1	5.6	0.81
NumOfSegments	19.0	13.8	14.7	10.9	0.81
NumBranchPoints	7.4	6.6	5.2	4.8	0.80
MaxBranchLayer	1.5	0.8	2.5	1.0	0.75
Area	2738.0	641.8	2364.2	632.0	0.74
Lvl1TotLength	715.3	398.8	640.3	350.2	0.72
Perimeter	168.0	21.0	214.8	30.6	0.71
Mean tert length	11.9	16.1	26.4	47.9	0.68
Lvl3MaxLength	24.0	43.8	66.9	154.6	0.68
Lvl2TotLength	331.5	426.7	361.3	402.3	0.65
Lvl3NoBranches	1.5	2.5	2.1	4.7	0.63
Mean primary length	189.6	106.1	169.0	84.1	0.61
Lvl1MaxLength	404.7	290.4	359.2	237.4	0.60
Lvl2NoBranches	5.7	4.2	3.6	2.8	0.59
MeanBranchLayer	0.8	0.5	1.4	0.4	0.58
Lvl2MaxLength	121.8	138.8	196.1	229.0	0.58
Mean sec length	47.0	37.1	88.6	83.9	0.51

Neurite structure irrelevant descriptors are highlighted.

The Pearson's correlation coefficients larger than 0.9 are in bold.

3.2 Ability to Characterize Neurite Branching

Ability of HCA-Vision to characterize neurite branching was validated with Sez-6 image dataset [13]. The dataset includes a wild-type class (Pos) and a Sez-6 knockout class (Min), consisting of 96 images totally. Only 101 neurons in these images were selected for quantification (Fig. 36 (a), (b)). They semi-automatically annotated Sez-6 dataset with NeuronJ [10], and 17 morphological features were exported. There were statistical differences in 9 of these features about neurite branching. HCA-Vision got the same result as the semi-automatic annotation.

With the same set of parameters, we process all the neuron images of the two classes and generate neuronal morphology descriptors for the 101 neurons with NeurphologyS (Fig. 36 (c), (d)). Table 11 shows the mean value and standard deviation of each descriptor of Pos class and Min class, respectively. Besides, for each descriptor, Student's t-test is applied between the two classes to derive the p-value.

(a) Wild-type (b) Sez-6 Knockout

(c) Wild-type (d) Sez-6 Knockout

Fig. 36 Example result images of the two methods on Sez-6 dataset.

(a)(b) Result images of HCA-Vision. (c)(d) Corresponding result images of NeurphologyS.

Table 11 Quantification results of Sez-6 dataset with NeurphologyS.

Descriptors	Pos		Min		
	Mean	STDV	Mean	STDV	P-Value
Area	3230.9	996.5	3150.3	1085.2	0.6984
Perimeter	189.5	38.0	184.8	40.4	0.5494
TotalNeuriteLength	1547.0	648.2	1631.2	765.7	0.5530
MaxNeuriteLength	553.2	250.3	427.5	220.2	****0.0086**
MaxBranchLayer	2.7	0.7	1.8	0.5	0.7715
MeanBranchLayer	1.7	0.2	0.8	0.3	0.7505
NumBranchPoints	8.9	5.0	12.4	7.2	****0.0053**
NumOfRoots	5.7	1.6	6.9	2.3	****0.0030**
NumOfSegments	23.6	10.6	32.3	15.8	****0.0016**
NumOfExtremities	13.1	5.4	16.3	6.2	****0.0074**
NeuriteFieldArea	163886	106251	131063	84738	0.0890
MaxIntensity_Neurite	162.5	54.6	158.5	60.8	0.7258
MeanIntensity_Neurite	50.7	12.6	44.7	12.4	***0.0175**
IntegratedIntensity_Neurite	80177	43210	74887	43497	0.5
StdevIntensity_Neurite	28.8	9.3	26.3	6.9	0.1379
Lvl1NoBranches	5.7	1.6	6.9	2.3	****0.0030**
Lvl1TotLength	1023.2	345.3	1030.1	395.6	0.9260
Lvl1MaxLength	553.2	250.3	427.5	220.2	****0.0086**
Lvl2NoBranches	7.4	3.8	10.3	5.4	****0.0018**
Lvl2TotLength	474.1	329.0	539.2	350.1	0.3382
Lvl2MaxLength	156.7	127.8	130.8	85.8	0.2336
Lvl3NoBranches	1.4	1.9	2.1	2.3	0.1033
Lvl3TotLength	46.9	67.2	61.6	93.4	0.3646
Lvl3MaxLength	28.5	38.2	28.2	28.8	0.9657
MaxIntensity_Neuron	228.6	37.4	227.0	34.6	0.8252
MeanIntensity_Neuron	120.3	25.5	113.0	23.7	0.1376
IntegratedIntensity_Neuron	394668	153730	363061	162540	0.3
StdevIntensity_Neuron	49.5	8.5	48.2	8.5	0.4266
Mean primary length	188.0	76.6	153.3	47.9	****0.0077**
Mean sec length	65.6	43.3	50.8	17.5	***0.0277**
Mean tert length	21.5	26.7	21.5	19.8	0.9952

Descriptors with statistical difference that reported in HCA-Vision are highlighted.

Descriptors exported with NeuronJ are in bold.

The p-values of Student's t-test smaller than 0.05 are in bold.

*p<0.05, **p<0.01

In agreement with the results presented in report of HCA-Vision, the statistical results generated by NeurphologyS show statistical differences (p-value < 0.05) in 11 features. Nine of these features showed statistical differences in both semi-automatic results and HCA-Vision results. And, since number of segments and mean neurite intensity cannot be quantified with NeuronJ, only the results of HCA-Vision are available for the two features. We get statistical differences in the 2 features also.

Hence, the same conclusion as HCA-Vision can be made that knockout of Sez-6 exhibits excessive neurite branching, and the neurite structure discriminating ability of NeurphologyS is ensured.

3.3 Performance of Neurite Structure Features

Semi-automatic neurite tracing and branch order assignment of the GFP dataset is made by a neuroscientist with NeuronJ [10] for each of the 41 neurons (Fig. 37). To measure the performance of neurite structure feature extraction and quantification of NeurphologyS, we compare the correlation of NeurphologyS results and HCA-Vision results with the semi-automatic results.

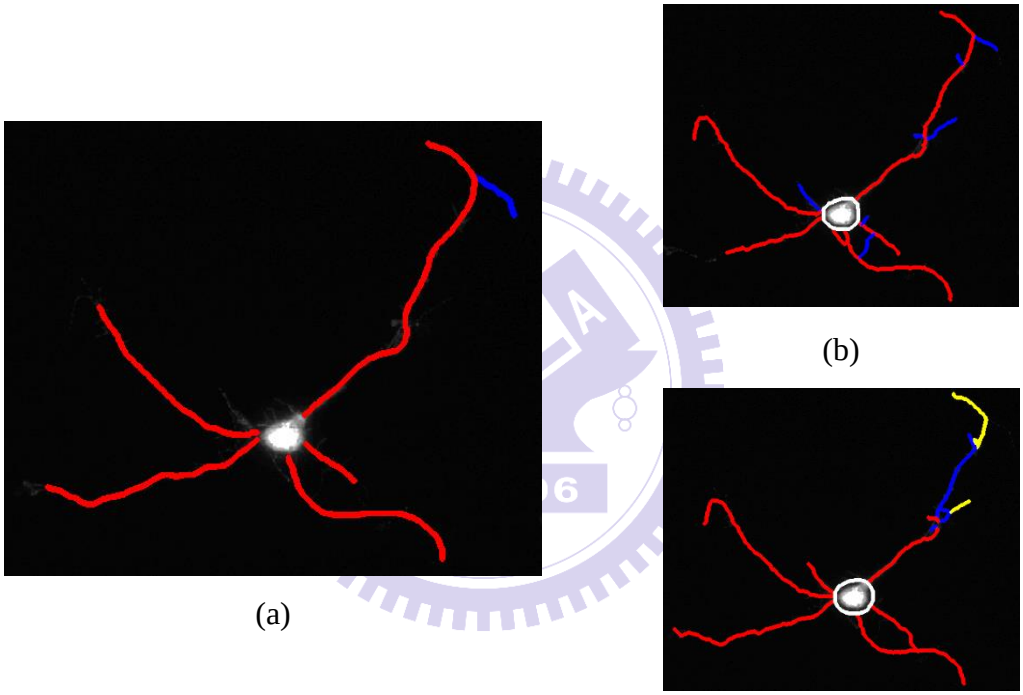

(a) (b) (c)

Fig. 37 Example annotation result on GFP dataset.

(a) Semi-automatic result. (b) NeurphologyS result. (c) HCA-Vision result.

The neuronal morphology descriptors that can be directly derived from NeuronJ are showed in Table 12. In addition to the mean and standard deviation of semi-automatic tracing results, Pearson's correlation coefficients are calculated between results generated manually and that of NeurphologyS and HCA-Vision, respectively.

Table 12 Semi-automatic quantification results of GFP dataset.

	Semi-automatic		Correlation	
Descriptors	**Mean**	**STDV**	**NeurphologyS**	**HCA-Vision**
Sum Len	1112.2	914.7	**0.98**	**0.91**
Max Len	495.0	444.4	**0.90**	0.86
Lv1 No	3.5	1.2	0.73	0.66
Lv1 Tot	850.8	567.2	**0.95**	0.61
Lv1 Max	495.0	444.4	0.89	0.55
Lv2 No	1.3	1.4	0.58	0.53
Lv2 Tot	228.7	356.7	**0.94**	0.57
Lv2 Max	124.5	161.8	0.89	0.50
Lv3 No	0.2	0.6	0.70	0.64
Lv3 Tot	32.8	84.3	0.78	0.61
Lv3 Max	26.2	66.9	**0.93**	0.56
Lv1 Mean	248.3	164.0	0.86	0.40
Lv2 Mean	92.6	103.6	0.75	0.64
Lv3 Mean	23.0	58.3	0.75	0.55

Descriptors with higher correlation to semi-automated result are highlighted.
The Pearson's correlation coefficients larger than 0.9 are in bold.

From the table, it is shown that the results of NeurphologyS acquire higher correlation with semi-automated results than HCA-Vision. NeurphologyS can perform well compared to HCA-Vision in mimicking annotation of human experts. Since we have compared performance of basic neuronal morphology detection, the main difference between the two methods will lie in branch order assignment.

In HCA-Vision, only average neurite intensity is considered when constructing neurite tree and deciding the branch priority. However, ignorance of neurite length will lead to preference of short, high-intensity neurite segments (Fig. 38 (c), (f)). The RANBO method devised for neurite tree growing and neurite branch priority decision employs local neurite angle as well as neurite subtree length. Hence, a smooth, long neurite with many branches is preferred, and this is closer to what we expected to be a neurite with high priority (Fig. 38 (b)). Since NeurphologyS decides the priority more

globally than HCA-Vision, this accounts for the high correlation in secondary neurite length. But the adoption of subtree length in branch priority decision can result in mistakes due to disturbance of noise (Fig. 38 (e)).

As in (Fig. 38 (g), (h), (i)), it can be shown that the neurite detection result of NeurphologyS is closer to semi-automatic method than that of HCA-Vision. This might result from the differences in method of neurite gap closing. And this can explain why NeurphologyS gets higher correlation in total or maximal neurite length.

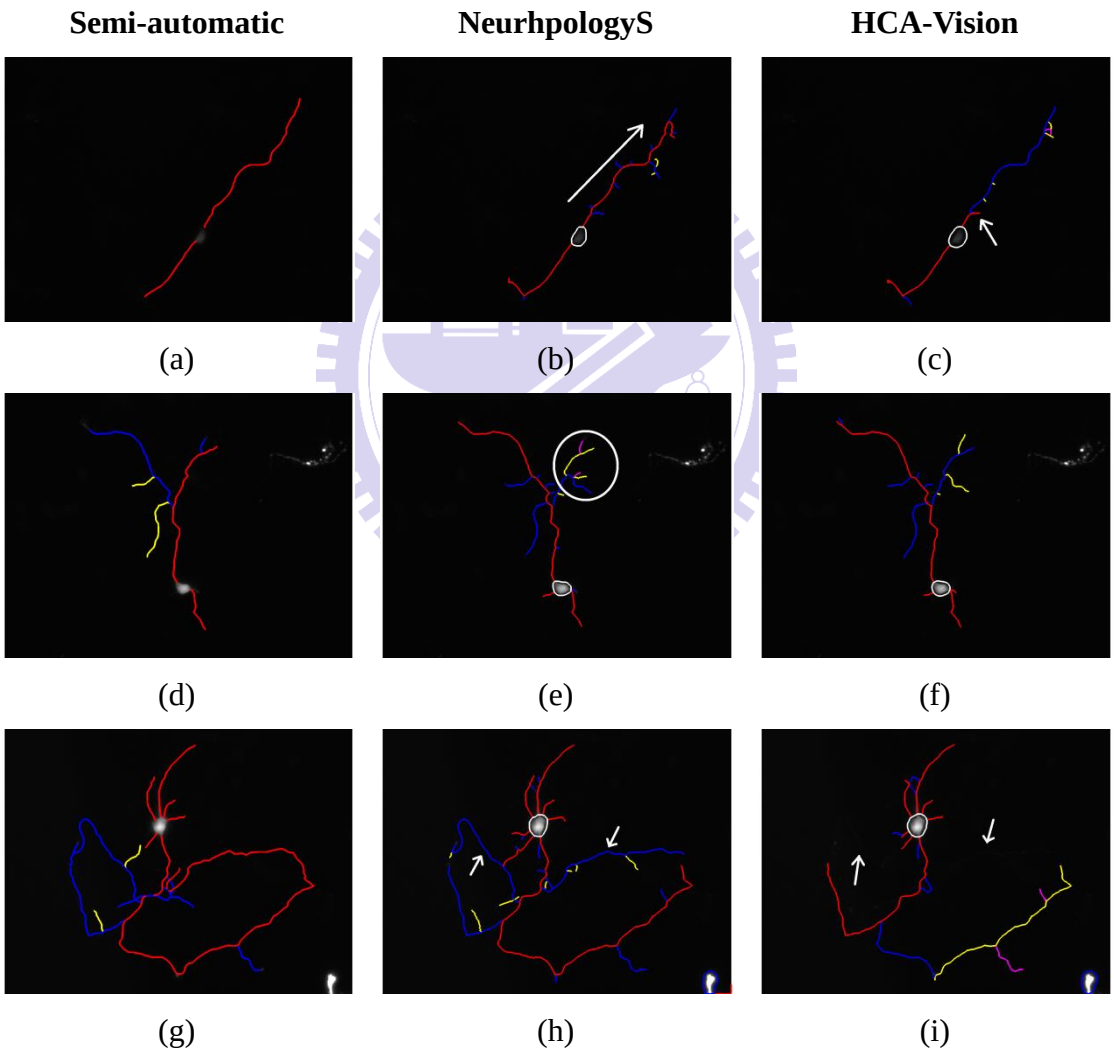

Fig. 38 Example results of GFP dataset.

Images in a row are results of the same neuron image with different methods. (a)(b)(c) Global branch decision making of our method. (d)(e)(f) Disturbance of noise to our method. (g)(h)(i) Our method extracts neurite closer to semi-automatic result.

CHAPTER 4

CONCLUSIONS AND FUTURE WORKS

4.1 Conclusions

The flourishing development of fluorescent microscopy benefits acquisition of massive neuron image dataset. Owing to the crucial role play by neuronal morphologies in neuroscience, numerous applications proved their versatile ability. Out of these features, neurite structure descriptors characterize neurite branching well. However, there are few studies aiming at extraction of neurite structure descriptor.

Thus, in this thesis, we propose an automated system, NeurphologyS, for extraction and quantification of morphological features from neuron images, including neurite structure. The system consists of basic neuronal morphology detection and a proposed rule-based neurite tree growing and backward branch priority decision (RANBO) method for the task of neurite structure extraction. NeurphologyS is freely available, open-source and cross-platform with MATLAB implemented GUI.

The correctness, ability to characterize neurite branch and performance of extracted neurite structure descriptor are evaluated with two neuron image datasets. It can be known from the results that NeurphologyS performs well compared to the outstanding commercial software, HCA-Vision. Resulted from the RANBO method, NeurphologyS can generate quantification results that get higher correlation with semi-automatic tracing results annotated by human experts.

4.2 Future Works

Although the proposed RANBO method endeavors to simulate the behavior of human annotator, only simplified concept with local neurite segment angles are considered to solve neurite crossovers in 2D neuron images. Due to the complexity of neurite growth, RANBO cannot solve all the situations encountered perfectly.

For the neurite tree growing task, more elaborated techniques can be designed for analyzing the complex neurite anatomy. Other conditions, such as intensity, curve smoothness or global trend of neurite, etc., can be integrated to construct a more robust and reliable tree growing result.

And for the neurite branch priority decision, only one single feature, the total subtree length, is utilized in the backward branch priority decision, it is possible and heuristic that multiple features can be combined to generate results mimicking expert operators well. The backward property makes it possible to include more global features, such information of the whole parent neurite and the whole subtree thereafter of the current bifurcation points.

NeurphologyS can quantify 53 morphological features including neurite structure descriptors. Since we cannot predict all the morphological differences caused by experimental modulation. It is necessary to incorporate more morphological features for describing the neuron cell.

Analysis of advanced neuronal morphology, such as neurite structure, is highly limited by complex neurite outgrowth. The performance of NeurphologyS on densely stained neuron cultures cannot be ensured. However, a more global quantification about a whole neuron image instead of individual neurons is also necessary. A robust tool capable of quantify advanced neuronal morphologies among densely stained neuron population will be powerful and can be used in much more situations.

REFERENCES

[1] T. Debeir, J. Benavides, and X. Vigé, "Involvement of protease-activated receptor-1 in the in vitro development of mesencephalic dopaminergic neurons.," *Neuroscience,* vol. 82, pp. 739-52, Feb 1998.

[2] E. W. Dent, A. M. Barnes, F. Tang, and K. Kalil, "Netrin-1 and semaphorin 3A promote or inhibit cortical axon branching, respectively, by reorganization of the cytoskeleton," *J Neurosci,* vol. 24, pp. 3002-12, Mar 24 2004.

[3] J. Jaworski, S. Spangler, D. P. Seeburg, C. C. Hoogenraad, and M. Sheng, "Control of dendritic arborization by the phosphoinositide-3'-kinase-Akt-mammalian target of rapamycin pathway," *J Neurosci,* vol. 25, pp. 11300-12, Dec 7 2005.

[4] R. E. van Kesteren, C. Carter, H. M. Dissel, J. van Minnen, Y. Gouwenberg, N. I. Syed, *et al.*, "Local synthesis of actin-binding protein beta-thymosin regulates neurite outgrowth," *J Neurosci,* vol. 26, pp. 152-7, Jan 4 2006.

[5] T. Houchin-Ray, L. A. Swift, J. H. Jang, and L. D. Shea, "Patterned PLG substrates for localized DNA delivery and directed neurite extension," *Biomaterials,* vol. 28, pp. 2603-11, Jun 2007.

[6] T. S. Gertler, C. S. Chan, and D. J. Surmeier, "Dichotomous anatomical properties of adult striatal medium spiny neurons," *J Neurosci,* vol. 28, pp. 10814-24, Oct 22 2008.

[7] A. Dall'Oglio, G. Gehlen, M. Achaval, and A. A. Rasia-Filho, "Dendritic branching features of Golgi-impregnated neurons from the "ventral" medial amygdala subnuclei of adult male and female rats," *Neurosci Lett,* vol. 439, pp. 287-92, Jul 18 2008.

[8] J. Betts-Henderson, S. Bartesaghi, M. Crosier, S. Lindsay, H. L. Chen, P. Salomoni, *et al.*, "The nystagmus-associated FRMD7 gene regulates neuronal outgrowth and development," *Hum Mol Genet,* vol. 19, pp. 342-51, Jan 15 2010.

[9] R. S. O'Dell, C. J. Ustine, D. A. Cameron, S. M. Lawless, R. M. Williams, W. R. Zipfel, *et al.*, "Layer 6 cortical neurons require Reelin-Dab1 signaling for cellular orientation, Golgi deployment, and directed neurite growth into the marginal zone," *Neural Dev*, vol. 7, p. 25, 2012.

[10] E. Meijering, M. Jacob, J. C. Sarria, P. Steiner, H. Hirling, and M. Unser, "Design and validation of a tool for neurite tracing and analysis in fluorescence microscopy images," *Cytometry A*, vol. 58, pp. 167-76, Apr 2004.

[11] S. L. Wearne, A. Rodriguez, D. B. Ehlenberger, A. B. Rocher, S. C. Henderson, and P. R. Hof, "New techniques for imaging, digitization and analysis of three-dimensional neural morphology on multiple scales," *Neuroscience*, vol. 136, pp. 661-80, 2005.

[12] M. L. Narro, F. Yang, R. Kraft, C. Wenk, A. Efrat, and L. L. Restifo, "NeuronMetrics: software for semi-automated processing of cultured neuron images," *Brain Res*, vol. 1138, pp. 57-75, Mar 23 2007.

[13] P. Vallotton, R. Lagerstrom, C. Sun, M. Buckley, D. Wang, M. De Silva, *et al.*, "Automated analysis of neurite branching in cultured cortical neurons using HCA-Vision," *Cytometry A*, vol. 71, pp. 889-95, Oct 2007.

[14] M. Pool, J. Thiemann, A. Bar-Or, and A. E. Fournier, "NeuriteTracer: a novel ImageJ plugin for automated quantification of neurite outgrowth," *J Neurosci Methods*, vol. 168, pp. 134-9, Feb 15 2008.

[15] J. Cheng, X. Zhou, E. Miller, R. M. Witt, J. Zhu, B. L. Sabatini, *et al.*, "A novel computational approach for automatic dendrite spines detection in two-photon laser scan microscopy," *J Neurosci Methods*, vol. 165, pp. 122-34, Sep 15 2007.

[16] J. J. Leandro, R. M. Cesar-Jr, and F. Costa Lda, "Automatic contour extraction from 2D neuron images," *J Neurosci Methods*, vol. 177, pp. 497-509, Mar 15 2009.

[17] W. Yu, H. K. Lee, S. Hariharan, W. Bu, and S. Ahmed, "Quantitative neurite outgrowth measurement based on image segmentation with topological dependence," *Cytometry A*, vol. 75, pp. 289-97, Apr 2009.

[18] C. Wu, J. Schulte, K. J. Sepp, J. T. Littleton, and P. Hong, "Automatic robust neurite detection and morphological analysis of neuronal cell cultures in high-content screening," *Neuroinformatics,* vol. 8, pp. 83-100, Jun 2010.

[19] S. Y. Ho, C. Y. Chao, H. L. Huang, T. W. Chiu, P. Charoenkwan, and E. Hwang, "NeurphologyJ: an automatic neuronal morphology quantification method and its application in pharmacological discovery," *BMC Bioinformatics,* vol. 12, p. 230, 2011.

[20] L. Dehmelt, G. Poplawski, E. Hwang, and S. Halpain, "NeuriteQuant: an open source toolkit for high content screens of neuronal morphogenesis," *BMC Neurosci,* vol. 12, p. 100, 2011.

[21] I. Rishal, O. Golani, M. Rajman, B. Costa, K. Ben-Yaakov, Z. Schoenmann, *et al.,* "WIS-NeuroMath enables versatile high throughput analyses of neuronal processes," *Dev Neurobiol,* vol. 73, pp. 247-56, Mar 2013.

[22] J. A. Mitchel, I. S. Martin, and D. Hoffman-Kim, "Neurient: an algorithm for automatic tracing of confluent neuronal images to determine alignment," *J Neurosci Methods,* vol. 214, pp. 210-22, Apr 15 2013.

[23] L. Billeci, C. Magliaro, G. Pioggia, and A. Ahluwalia, "NEuronMOrphological analysis tool: open-source software for quantitative morphometrics," *Front Neuroinform,* vol. 7, p. 2, 2013.

[24] E. Meijering, M. Jacob, J. C. F. Sarria, P. Steiner, H. Hirling, and M. Unser, "Neurite tracing in fluorescence microscopy images using ridge filtering and graph searching: principles and validation," Proc IEEE Int Symp Biomed Imaging, vol. 2, pp. 1219-1222, Arlington, VA, USA, 2004.

[25] J. M. Gunnersen, M. H. Kim, S. J. Fuller, M. De Silva, J. M. Britto, V. E. Hammond, *et al.,* "Sez-6 proteins affect dendritic arborization patterns and excitability of cortical pyramidal neurons," *Neuron,* vol. 56, pp. 621-39, Nov 21 2007.

[26] J. S. Weszka and A. Rosenfeld, "Histogram Modification for Threshold Selection," *IEEE Trans. Syst., Man, Cybern.,* vol. 9, pp. 38-52, 1979.

[27] R. Lagerstrom and M. Buckley, "A graph watershed method for analysis and quantification of neurite branching structure," 18th World IMACS/MODSIM Congress, pp. 762-767, Cairns, Australia, 2009.

[28] D. Wang, R. Lagerstrom, C. Sun, L. Bishof, P. Valotton, and M. Gotte, "HCA-vision: Automated neurite outgrowth analysis," *J Biomol Screen*, vol. 15, pp. 1165-70, Oct 2010.

[29] R. C. Gonzalez and R. E. Woods, *Digital Image Processing (3rd Edition)*. Upper Saddle River, NJ, USA: Prentice-Hall, Inc., 2006.

[30] C. Sun and P. Vallotton, "Fast Linear Feature Detection Using Multiple Directional Non-Maximum Suppression," 18th Int. Conf. Pattern Recognition (ICPR), vol. 2, pp. 288-291, Hong Kong, 2006.

[31] M. A. Olsen, D. Hartung, C. Busch, and R. Larsen, "Convolution approach for feature detection in topological skeletons obtained from vascular patterns," IEEE Workshop on Computational Intelligence in Biometrics and Identity Management (CIBIM), pp. 163-167, Paris, France, 2011.